frontiers | Frontiers in Marine Science

TYPE Original Research
PUBLISHED 11 January 2024
DOI 10.3389/fmars.2023.1320655



OPEN ACCESS

EDITED BY
Glen T. Snyder,
The University of Tokyo, Japan

REVIEWED BY
Natascha Riedinger,
Oklahoma State University, United States
Satoko Owari,
Tokyo University of Marine Science and Technology, Japan

*CORRESPONDENCE
Desiree L. Roerdink
desiree.roerdink@uib.no

RECEIVED 12 October 2023
ACCEPTED 26 December 2023
PUBLISHED 11 January 2024

CITATION
Roerdink DL, Vulcano F, Landro J-K, Moltubakk KE, Babel HR, Jørgensen SL, Baumberger T, Økland IE, Reeves EP, Thorseth IH, Reigstad LJ, Strauss H and Steen IH (2024) Hydrothermal activity fuels microbial sulfate reduction in deep and distal marine settings along the Arctic Mid Ocean Ridges.
*Front. Mar. Sci.* 10:1320655.
doi: 10.3389/fmars.2023.1320655



# Hydrothermal activity fuels microbial sulfate reduction in deep and distal marine settings along the Arctic Mid Ocean Ridges

Desiree L. Roerdink[1]*, Francesca Vulcano[2], Jan-Kristoffer Landro[1], Karen E. Moltubakk[1], Hannah R. Babel[2], Steffen Leth Jørgensen[1,2], Tamara Baumberger[1,3], Ingeborg E. Økland[1], Eoghan P. Reeves[1], Ingunn H. Thorseth[1], Laila J. Reigstad[2], Harald Strauss[4] and Ida H. Steen[2]

[1]Department of Earth Science and Centre for Deep Sea Research, University of Bergen, Bergen, Norway, [2]Department of Biological Sciences and Centre for Deep Sea Research, University of Bergen, Bergen, Norway, [3]Pacific Marine Environmental Laboratory, National Oceanographic and Atmospheric Administration & Cooperative Institute for Marine Ecosystem and Resources Studies, Oregon State University, Newport, OR, United States, [4]Institute for Geology and Paleontology, Westfälische Wilhelms-Universität Münster, Münster, Germany

Microbial sulfate reduction is generally limited in the deep sea compared to shallower marine environments, but cold seeps and hydrothermal systems are considered an exception. Here, we report sulfate reduction rates and geochemical data from marine sediments and hydrothermal vent fields along the Arctic Mid Ocean Ridges (AMOR), to assess the significance of basalt-hosted hydrothermal activity on sulfate reduction in a distal deep marine setting. We find that cored marine sediments do not display evidence for sulfate reduction, apart from low rates in sediments from the Knipovich Ridge. This likely reflects the overall limited availability of reactive organic matter and low sedimentation rates along the AMOR, except for areas in the vicinity of Svalbard and Bear Island. In contrast, hydrothermal samples from the Seven Sisters, Jan Mayen and Loki's Castle vent fields all demonstrate active microbial sulfate reduction. Rates increase from a few 10s to 100s of pmol $SO_4^{2-}$ $cm^{-3}$ $d^{-1}$ in active high-temperature hydrothermal chimneys, to 10s of nmol $SO_4^{2-}$ $cm^{-3}$ $d^{-1}$ in low-temperature barite chimneys and up to 110 nmol $cm^{-3}$ $d^{-1}$ in diffuse venting hydrothermal sediments in the Barite field at Loki's Castle. Pore fluid and sediment geochemical data suggest that these high rates are sustained by organic compounds from microbial mats and vent fauna as well as methane supplied by high-temperature hydrothermal fluids. However, significant variation was observed between replicate hydrothermal samples and observation of high rates in seemingly inactive barite chimneys suggests that other electron donors may be important as well. Sediment sulfur isotope signatures concur with measured rates in the Barite field and indicate that microbial sulfate reduction has occurred in the hydrothermal sediments since the recent geological past.

Our findings indicate that basalt-hosted vent fields provide sufficient electron donors to support microbial sulfate reduction in high- and low-temperature hydrothermal areas in settings that otherwise show very low sulfate reduction rates.

KEYWORDS

microbial sulfate reduction, hydrothermal chimneys, hydrothermal sediment, marine sediment, spreading ridges, rift valley, radiotracer rates, sulfur isotopes

## 1 Introduction

Sulfate reduction is a widespread microbial metabolism in marine sediments (e.g. Goldhaber and Kaplan, 1975; Jørgensen, 1982; Canfield, 1991; Jørgensen et al., 2019). Dissimilatory sulfate-reducing bacteria and archaea obtain energy from the reduction of sulfate ($SO_4^{2-}$) linked to the oxidation of electron donors such as molecular hydrogen, methane or organic acids such as acetate, lactate and pyruvate that are produced by biological degradation of organic matter (Jørgensen and Kasten, 2006). This metabolic coupling with carbon implies that microbial sulfate reduction plays an important role in the global carbon cycle, and estimates suggest that the annual global reduction of 11.3 teramoles of sulfate is responsible for the oxidation of 11-29% of the organic carbon flux to the seafloor (Bowles et al., 2014). The highest activities of sulfate reducers (up to several 100s of nmol $SO_4^{2-}$ $cm^{-3}$ $d^{-1}$) are typically observed in near-shore shallow marine environments (e.g. Howarth and Jørgensen, 1984; Moeslundi et al., 1994; Thamdrup et al., 1994), where an optimum balance between high sedimentation rates and high primary productivity enables the preservation of organic matter after consumption by oxic respiration (Berner, 1978; Canfield, 1991). In contrast, sediments on the continental rise (2000-3500 m depth) and abyssal plains (>3500 m depth) are typically poor in organic matter, and calculated depth-integrated sulfate reduction rates are one to four orders of magnitude lower than for organic-rich shelf environments (Bowles et al., 2014).

Sedimented hydrothermal vent fields on oceanic spreading ridges have been shown to represent an exception to low microbial sulfate reduction rates found in deep sea settings. Organic-rich hydrothermal sediments in the Guaymas Basin (2000 m depth, Gulf of California) exhibit very high sulfate reduction rates of up to 1560 nmol $SO_4^{2-}$ $cm^{-3}$ $d^{-1}$ (Jørgensen et al., 1990; Elsgaard et al., 1994; Kallmeyer and Boetius, 2004), and rates in the hydrothermal sediments of Middle Valley (2430 m depth, Juan de Fuca Ridge) range up to 100 nmol $SO_4^{2-}$ $cm^{-3}$ $d^{-1}$ (Wankel et al., 2012). In addition, high sulfate reduction rates of up to 1000s of nmol $SO_4^{2-}$ $cm^{-3}$ $d^{-1}$ were measured in actively venting sulfide deposits at Middle Valley (Frank et al., 2013) and a hydrothermal flange at the sediment-influenced Main Endeavour vent field on the Juan de Fuca Ridge (2220 m depth) (Frank et al., 2015). The importance of sulfate reducers in these sedimented hydrothermal systems has been explained by the abundance of sulfate and electron donors resulting from the mixing of reduced hydrothermal fluids and oxidized seawater, as well as the chemosynthetic production of organic carbon (Jannasch and Mottl, 1985; Jørgensen et al., 1990; McCollom and Shock, 1997; Frank et al., 2013). However, the majority of hydrothermal vent fields worldwide occurs on bare volcanic rocks with no or minimal sediment cover (Beaulieu and Szafranski, 2020), and are characterized by high-temperature fluids with lower pH, $CH_4$ and $H_2$ concentrations than sediment-associated systems (Baumberger et al., 2016b). In addition, non-hydrothermal sediments surrounding deep sea vent fields typically show very low sulfate reduction rates (cf. Bowles et al., 2014), in contrast to the Guaymas Basin where organic-rich sediments yield rates of up to 11.8 nmol $SO_4^{2-}$ $cm^{-3}$ $d^{-1}$ (Elsgaard et al., 1994). Therefore, to better evaluate the importance of microbial sulfate reduction in hydrothermal systems on global oceanic spreading ridges, additional data is required from geological settings with bare-rock hydrothermal vent sites.

Here, we investigate the significance of hydrothermal activity on microbial sulfate reduction along the Arctic Mid Ocean Ridges (AMOR) in the Norwegian-Greenland Sea. The large variation in water depth, sedimentation rates and hydrothermal geochemistry enables us to compare sulfate reduction rates from marine sediments obtained from rift valleys with hydrothermal systems that cover a range of environmental conditions. We explore high- and low-temperature hydrothermal chimneys as well as hydrothermal sediments from basalt-hosted venting areas at Seven Sisters, Jan Mayen and sediment-influenced Loki's Castle, and evaluate ridge segment-scale variations in microbial sulfate reduction rates in background marine sediments. Our results reinforce those of previous studies showing elevated sulfate reduction rates in hydrothermal settings, and expand this to basalt-hosted systems without significant sediment cover.

## 2 Geological setting

The AMOR are a system of ultra-slow spreading ridges (full spreading rate 6-20 mm/year) that extends from the northern shelf of Iceland to the Siberian shelf in the Laptev Sea (Pedersen et al.,

2010b). Unlike volcanically active faster spreading ridges, the morphology of ultra-slow spreading ridges is characterized by broad axial rift valleys that are dominated by tectonics (Dick et al., 2003; Snow and Edmonds, 2007). The presence and exposure of ultramafic mantle rocks in these geological settings can generate methane and hydrogen through serpentinization reactions (Seyfried, 1987; Horita and Berndt, 1999; Cannat et al., 2010), resulting in hydrothermal vent sites with highly variable fluid compositions (Kelley et al., 2001; Edmonds et al., 2003; Baker et al., 2004; Pedersen et al., 2010a; Tao et al., 2012; Kinsey and German, 2013). Compared to faster spreading ridges, these hydrothermal systems may be active for longer periods of time and support distinct microbial communities (Nakamura and Takai, 2014; Ding et al., 2017; Lecoeuvre et al., 2021).

We focus on the part of the AMOR in the Norwegian-Greenland Sea that consists of the three segments Kolbeinsey Ridge (66.5 to 71.7°N), Mohns Ridge (70.9 to 73.6°N) and Knipovich Ridge (73.6 to 78.0°N) (Figure 1). Along this section, the rift valley floor is deepening towards the north from 1000 m at the hotspot-influenced Kolbeinsey Ridge to a maximum of 3500 m at the Knipovich Ridge. A sedimentation rate of 2-7 cm per 1000 years results in the accumulation of sediment within the rift valleys (Stein, 1990; Stubseid et al., 2023), in particular along the northernmost segments where the ridge is close to the Svalbard continental margin (Fiedler and Faleide, 1996). Glacigenic sediments from the Bear Island Fan reach the spreading ridge at the Mohns-Knipovich bend (Bruvoll et al., 2009).

Several high-temperature hydrothermal vent fields are located on the AMOR (Pedersen et al., 2010b; Pedersen and Bjerkgård, 2016), of which we focus on three in this study: Seven Sisters, Jan Mayen and Loki's Castle (Table 1). Seven Sisters is a shallow hydrothermal vent field (120 m depth) that occurs in mafic volcaniclastic rocks on top of a flat-topped volcano on the Kolbeinsey Ridge (Marques et al., 2020). Fluids of up to 200°C vent from barite and anhydrite-rich structures and are low in metals, $CH_4$ and $H_2$ (Marques et al., 2020) (Table 1). The Jan Mayen vent fields are situated on the southern Mohns Ridge at a depth of 550-700 meters (Pedersen et al., 2005), and consist of the Troll Wall, Soria Moria and Perle & Bruse venting areas. This study concentrates on the basalt-hosted Perle & Bruse field, which is located at 580 m depth at the flank of a large volcano that is undergoing rifting (Pedersen and Bjerkgård, 2016). Sulfide-rich chimneys vent fluids of up to 270°C with higher $CH_4$ concentrations than at Seven Sisters (Dahle et al., 2018) (Table 1). Loki's Castle vent field occurs at 2300 m depth on the northernmost section of the Mohns Ridge at the Mohns-Knipovich bend (Pedersen et al., 2010a). High-temperature (up to 315°C) fluids with high concentrations of $NH_4^+$, $H_2$ and $CH_4$ at Loki's Castle indicate a sedimentary influence to the basalt-hosted hydrothermal system (Baumberger et al., 2016a; Baumberger et al., 2016b). Adjacent to the high-temperature venting site is a circa 50 by 50 m area (Barite field) with low-temperature (20°C) barite chimneys and diffuse venting from sediments that are covered with microbial mats (Pedersen et al., 2010a; Steen et al., 2016). Previous work has suggested an important role for microbial sulfate reduction in and below the Barite field based on sulfur isotope signatures and sequencing data (Eickmann et al., 2014; Steen et al., 2016).

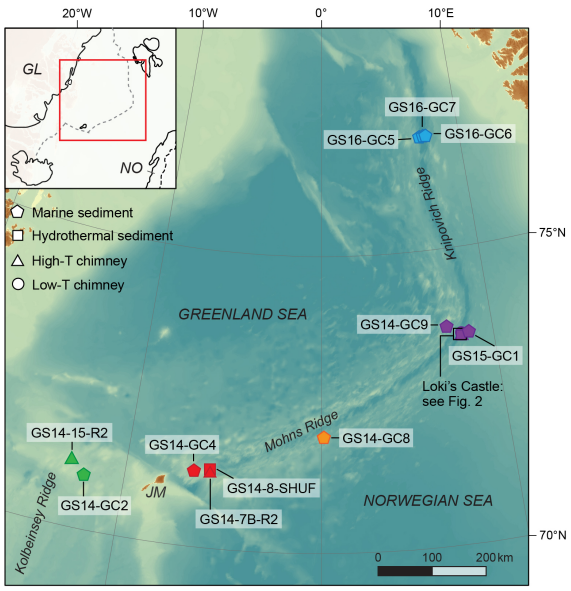


FIGURE 1
The Arctic Mid Ocean Ridge system (AMOR) and the island of Jan Mayen (JM) with locations of sampled marine sediments (diamonds), hydrothermal sediments (squares), high-temperature chimneys (triangles) and low-temperature chimneys (circles). Inset shows the location of the AMOR (dashed grey line) relative to Greenland (GL) and Norway (NO), and the location of the map (red box). Map created with ArcGIS using Ocean Basemap.

# 3 Materials and methods

## 3.1 Samples

Samples were collected during five research cruises with R/V G.O. Sars, using gravity coring equipment for marine sediments and ROV Ægir 6000 for hydrothermal chimneys, deposits and sediments (Table 2).

### 3.1.1 Kolbeinsey Ridge

One anhydrite-sulfide rich hydrothermal chimney sample was collected from the actively venting Lily mound at Seven Sisters vent field (GS14-15-R02). In addition, a 2.2 m long gravity core (GS14-GC2) was collected from the nearest sedimented basin to the ridge, approximately 40 km southeast of the Seven Sisters vent field (Figure 1). No hydrothermal sediments were obtained from this location.

### 3.1.2 Mohns Ridge

Four sediment cores were collected from rift flanks along the Mohns Ridge (Figure 1). One core (GS14-GC4) was sampled on the southern end of the Mohns Ridge, circa 30 km west of the Jan Mayen vent field on the western rift flank. Another core was collected along the central part of the Mohns Ridge (GS14-GC8)

TABLE 1 Hydrothermal vent fields investigated in this study.

| Vent field | Ridge | Host rock | Depth (m) | T (°C)[1] | pH[2] | $CH_4$ (μM) |
|---|---|---|---|---|---|---|
| Seven Sisters | Kolbeinsey | Basalt | 120 | 200 | 5.0 | 30 |
| Jan Mayen | S Mohns | Basalt | 580 | 270 | 4.7 | 5400 |
| Loki's Castle | N Mohns | Basalt, sediment[3] | 2361 | 315 | 5.6 | 14300 |

[1]Maximum measured in situ temperature. [2]Determined at 25°C. [3]Interaction with sediments at depth as inferred from fluid geochemistry. Data from Marques et al. (2020) for Lily mound, Seven Sisters; Dahle et al. (2018) for Bruse chimney, Jan Mayen; and Pedersen et al. (2010a); Baumberger et al. (2016b) for Camel chimney, Loki's Castle.

on the eastern flank. Sediment cores were also obtained from both rift flanks at the northern section of the Mohns Ridge near Loki's Castle hydrothermal vent field, with one core (GC14-GC9) taken in a sedimented basin on the Schulz Massif oceanic core complex and one core (GC15-GC1) in distal Bear Island Fan sediments, 5 km east of the rift valley.

Hydrothermal samples were collected from the Jan Mayen and Loki's Castle vent fields on the southern and northern end of the Mohns Ridge, respectively. One anhydrite-sulfide rich sample was obtained from the active Bruse chimney in the basalt-hosted Jan Mayen hydrothermal vent field (GS14-7B-R2), and hydrothermal sediments were collected from the nearby Perle chimney using a shuffle box with a shovel front (GS14-8-SHUF). A temperature of 70°C was measured in the hydrothermal sediments at circa 0.5 m depth. At Loki's Castle, five barite chimneys with different appearances were collected from the low-temperature (20°C) Barite field (Figure 2). Chimneys GS18-28-R6 and GS18-28-R8 are covered with white microbial mats and showed diffuse fluid venting, while chimney GS18-28-R3 is white and yellow-colored with no visible microbial mat, chimney GS15-9-R1 is yellow-colored and GS18-28-R5 is orange-colored (Supplementary Figure 1). Sediments from the Barite field were sampled in three different ways: a push core from the surface sediment layer (~10 cm) in between barite chimneys (GS15-9-PC2), a blade core (~20 cm) from active diffuse venting sediments below a microbial mat (GS18-28-BC3), and a gravity core (207 cm) that was deployed with a transponder to ensure correct positioning within the Barite field (GS14-GC14). One blade core was collected on the outer perimeter of the Barite field (GS18-28-BC4). In addition, one anhydrite-sulfide rich piece from the Camel chimney (GS18-22-R2) was obtained from the western high-temperature hydrothermal mound at Loki's Castle.

### 3.1.3 Knipovich Ridge

Three gravity cores were collected along an east-west transect on the central Knipovich Ridge (Figure 1), one on the western rift flank (GS16-GC5), one on the eastern rift flank (GS16-GC6) and one within the rift valley (GS16-GC7).

## 3.2 Methodology

### 3.2.1 Sulfate reduction rates

#### 3.2.1.1 Marine sediments

Immediately after splitting of the retrieved sediment cores, duplicate subsamples (4 $cm^3$) were collected at regular depth intervals using sterile plastic syringes without tips (Røy et al., 2014). Sediment samples were subsequently incubated in the on-board laboratory with 10 μL (185 kBq) of $^{35}SO_4^{2-}$ tracer (PerkinElmer) using a Hamilton syringe, sealed off with a butyl rubber stopper and placed in a $N_2$-filled sealable plastic bag. Based on measured bottom seawater temperatures of ~1°C, samples were incubated in the refrigerator at 4°C for 0.5 to 35 days depending on the expected range of sulfate reduction rates. Re-oxidation of sulfide was avoided by maintaining an anoxic atmosphere during the incubations, and 1 $cm^3$ of sediment was collected from each horizon and frozen to determine sediment porosity from the weight loss during drying for 3 days at 105°C. At the end of the incubation time, sediment samples were quantitatively transferred into 50 ml Falcon tubes with 5 ml 20% zinc acetate and frozen at -20°C to stop microbial activity. To assess background $^{35}S$ levels, duplicate sediment samples were transferred directly into 20% zinc acetate solutions without the addition of radiotracer. In addition, controls to determine distillation blanks were collected by adding $^{35}SO_4^{2-}$ and immediately transferring the radiolabeled sediments to 20% zinc acetate solutions.

#### 3.2.1.2 Hydrothermal sediments

Hydrothermal sediments and control samples were collected in a similar way to marine sediments using sterile plastic syringes, but a higher incubation temperature (20°C) was used for the samples collected from the Loki's Castle Barite field based on measured *in situ* sediment temperatures. Incubation times ranged from 0.8 to 3.1 days and control samples were collected to measure background $^{35}S$ and distillation blanks.

#### 3.2.1.3 Hydrothermal chimneys

High- and low-temperature hydrothermal chimneys were sampled promptly after recovery on board. Chimney fragments were quickly crushed into a slurry using a flame-sterilized steel mortar and pestle and immediately transferred to an anaerobic glove bag filled with $N_2$. A volume of 2.5 ml of slurry was added to an Exetainer vial, and 1.0 ml of fluid (sampled bottom seawater or artificial seawater) was added to represent *in situ* sulfate concentrations in the chimney, following the method by Frank et al. (2013). Samples were subsequently incubated with 10 μL (185 kBq) of $^{35}SO_4^{2-}$ tracer and Exetainers were flushed with $N_2$ gas to ensure anoxic conditions during incubation. Incubation was performed at 20°C for chimneys from the Loki's Castle Barite field, reflecting measured temperatures in the barite chimneys. High-temperature chimneys from the Seven Sisters and Jan Mayen vent fields were also incubated at 20°C during initial

10.3389/fmars.2023.1320655

TABLE 2 Overview of samples analyzed for microbial sulfate reduction rates, in order of increasing latitude.

| Sample name | Latitude | Longitude | Depth (m) | Description |
|---|---|---|---|---|
| Kolbeinsey Ridge | | | | |
| GS14-GC2 | 70°54.955'N | 12°02.202'W | 1036 | Marine sediment core (2.2 m) |
| GS14-15-R2 | 71°08.848'N | 12°47.482'W | 130 | Hydrothermal chimney (200°C) |
| Mohns Ridge | | | | |
| GS14-GC4 | 71°17.082'N | 06°33.696'W | 1050 | Marine sediment core (2.4 m) |
| GS14-7B-R2 | 71°17.897'N | 05°41.644'W | 594 | Hydrothermal chimney (270°C) |
| GS14-8-SHUF | 71°17.904'N | 05°42.257'W | 567 | Hydrothermal sediment |
| GS14-GC8 | 71°57.953'N | 00°06.142'E | 2476 | Marine sediment core (3.4 m) |
| GS18-28-R5 | 73°33.978'N | 08°09.726'E | 2361 | Hydrothermal barite chimney (20°C) |
| GS18-28-R8 | 73°33.978'N | 08°09.720'E | 2361 | Hydrothermal barite chimney (20°C) |
| GS15-9-PC2 | 73°33.981'N | 08°09.740'E | 2363 | Hydrothermal sediment |
| GS15-9-R1 | 73°33.981'N | 08°09.764'E | 2336 | Hydrothermal barite chimney (20°C) |
| GS18-28-BC3 | 73°33.984'N | 08°09.714'E | 2361 | Hydrothermal sediment |
| GS18-28-R3 | 73°33.984'N | 08°09.744'E | 2361 | Hydrothermal barite chimney (20°C) |
| GS18-28-R6 | 73°33.984'N | 08°09.726'E | 2361 | Hydrothermal barite chimney (20°C) |
| GS14-GC14 | 73°33.994'N | 08°09.686'E | 2330 | Hydrothermal sediment |
| GS18-22-R2 | 73°34.002'N | 08°09.402'E | 2310 | Hydrothermal chimney (315°C) |
| GS18-28-BC4 | 73°34.008'N | 08°09.738'E | 2361 | Hydrothermal sediment |
| GS15-GC1 | 73°34.533'N | 08°30.527'E | 2562 | Marine sediment core (3.9 m) |
| GS14-GC9 | 73°42.032'N | 07°20.659'E | 2653 | Marine sediment core (2.1 m) |
| Knipovich Ridge | | | | |
| GS16-GC5 | 76°54.766'N | 07°07.491'E | 3007 | Marine sediment core (3.6 m) |
| GS16-GC7 | 76°55.212'N | 07°23.371'E | 3493 | Marine sediment core (3.5 m) |
| GS16-GC6 | 76°55.253'N | 07°34.522'E | 2994 | Marine sediment core (0.9 m) |

Sample names include the year in which the sample was collected (GS13 to GS18) and the type of sampling equipment used, GC, gravity corer; PC, push corer; SHUF, shuffle box; BC, blade corer. For ROV-dives, the dive number is listed after AGR or ROV.

experiments due to a lack of suitable incubators on board, versus 80°C for the high-temperature chimney from Loki's Castle that was processed during a different cruise. After incubation, samples were quantitatively transferred into 50 ml Falcon tubes with 5 ml 20% zinc acetate and frozen at -20°C until further processing. Because of the heterogeneous nature of hydrothermal chimneys, each sample was measured at least in triplicate. Control slurries were treated in the same way as the sediments to obtain background $^{35}S$ values and distillation blanks.

#### 3.2.1.4 Radioactivity measurements

Thawed samples were centrifuged to separate supernatant with the remaining $^{35}SO_4^{2-}$ and solids with precipitated $Zn^{35}S$. A 100 µL aliquot was sampled from the supernatant and mixed with 5 ml 5% zinc acetate and 15 ml Ecoscint XR (National Diagnostics) scintillation fluid. Reduced sulfide was extracted from the sediments and crushed chimneys by cold chromium distillation (Canfield et al., 1986; Fossing and Jørgensen, 1989; Kallmeyer et al., 2004), collected in 5 ml 5% zinc acetate and mixed with 15 ml scintillation fluid. The activity of $^{35}S$ in the supernatant and reduced sulfide was subsequently counted for two times 20 minutes per sample using a PerkinElmer Tri-Carb 2900TR Liquid Scintillation Analyzer at the Department of Biological Sciences, University of Bergen, with an average detection limit of 34 counts per minute. No background $^{35}S$ was measured in any of the control samples and the carryover of $^{35}S$ from sulfate during distillation was negligible for marine sediments. Hydrothermal samples generally yielded a small but non-zero distillation blank of up to 58 counts per minute, and measured blank values were used to calculate blank-corrected activities.

#### 3.2.1.5 Sulfate reduction rate calculations

Sulfate reduction rates (in pmol $cm^{-3}$ $d^{-1}$) were calculated for the marine and hydrothermal sediments using the following equation:

$$SRR = [SO_4^{2-}]_{pf} \cdot \varphi_{sed} \cdot (a_{TRIS}/a_{TOTAL}) \cdot (1/t) \cdot 1.06 \cdot 10^6 \quad (1)$$

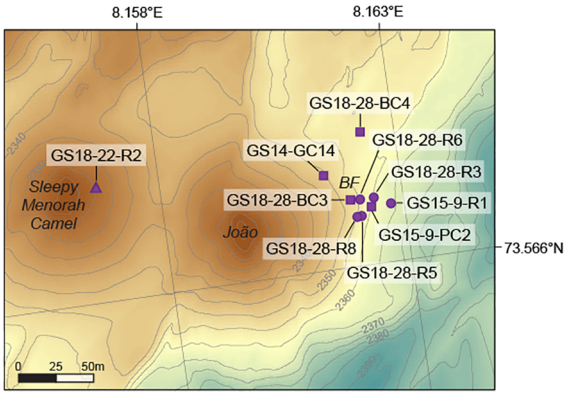


FIGURE 2
Detailed bathymetric map of the Loki's Castle vent field with all sample locations indicated (location of map area is shown in Figure 1). Sleepy, Menorah, Camel and Joao are high-temperature hydrothermal vents located on two hydrothermal mounds. The Barite field (BF) is located to the northeast of the eastern mound. Depth contours are given in meters. Symbols correspond to those used in Figure 1. Map created using ArcGIS.

where $[SO_4^{2-}]_{pf}$ is the measured sulfate concentration (mM) in pore waters at corresponding sediment depths (Section 3.2), $\varphi_{sed}$ is the measured sediment porosity, $a_{TRIS}$ is the blank-corrected radioactivity in the total reducible inorganic sulfur (TRIS), $a_{TOTAL}$ the total blank-corrected radioactivity in the sample, and $t$ the incubation time in days. No pore fluid sulfate profiles could be obtained for the blade cores, so that $[SO_4^{2-}]_{pf}$ was based on single measurements and assumed to be 23 mM for GS18-ROV28-BC3 and 28 mM for GS18-ROV28-BC4 for all horizons.

For the hydrothermal chimneys, sulfate reduction rates were calculated per volume of dry chimney material using a modified version of Equation 1. Firstly, the volume of chimney material in each sample ($V_{dry}$) was calculated using Equation 2:

$$V_{dry} = V_{slurry} \cdot (1 - \varphi_{slurry}) \quad (2)$$

where $V_{slurry}$ is the volume of the slurry (2.5 ml) and $\varphi_{slurry}$ is the porosity of the slurry. The total amount of sulfate present in each sample (in µmol) was calculated Equation 3:

$$SO_4^{2-}{}_{total} = ([SO_4^{2-}]_{slurry} \cdot \varphi_{slurry} \cdot V_{slurry} + [SO_4^{2-}]_{fluid} \cdot V_{fluid}) \quad (3)$$

where $[SO_4^{2-}]_{slurry}$ is the sulfate concentration of fluids naturally present in the slurry, here assumed to be similar to seawater (28 mM) due to flushing during transport from the seafloor, $[SO_4^{2-}]_{fluid}$ is the sulfate concentration in the added incubation fluids, and $V_{fluid}$ is the volume of incubation fluid added (1 ml). Sulfate reduction rates were subsequently calculated (in pmol $cm^{-3}$ $d^{-1}$) using Equation 4:

$$SRR = SO_4^{2-}{}_{total} \cdot (a_{TRIS}/a_{TOTAL}) \cdot (1/t) \cdot (1/V_{dry}) \cdot 1.06 \cdot 10^6 \quad (4)$$

The average detection limit for sulfate reduction rates is circa 5 pmol $cm^{-3}$ $d^{-1}$.

### 3.2.2 Pore fluid and sediment geochemistry

Pore fluids were sampled from sediment cores by vacuum extraction using 0.2 µm Rhizon filters and analyzed promptly for pH and alkalinity (Metrohm Titrando) on board. Ammonium, nitrate/nitrite, dissolved inorganic carbon, sulfide and phosphate were measured on board by a Quaatro continuous flow analyzer (Seal Analytical). Sulfate concentrations were determined on shore by ion chromatography (Metrohm) with a relative standard deviation of <4% on repeated analyses of a multi-element standard, and cations were analyzed in aliquots acidified to 2% $HNO_3$ by inductively coupled plasma atomic emission spectroscopy (Thermo Scientific iCap 7600 ICP-AES) with Sc as internal standard and repeated measurement of SPS-SW-2 (Spectrapure) for quality control (<5% relative standard deviation). In addition, sediment subsamples (2-5 $cm^3$) were mixed on board with artificial seawater and He for headspace extraction of dissolved $CH_4$ and analysis by gas chromatography using a TCD-FID detector (3-5% standard error).

Total organic carbon (TOC) contents and C/N ratios were determined in oven-dried (3 days at 105°C) and finely crushed sediment samples (30-50 mg). GS15 samples were analyzed by elemental analyzer with TIC module (Analytik Jena Multi EA 4000), where TOC was calculated from the difference between total carbon and total inorganic carbon contents. All other samples were reacted with 1 ml phosphoric acid to remove inorganic carbon and subsequently analyzed for TOC and C/N ratios by a Thermo Scientific Flash 1120 EA coupled to a Thermo Scientific Delta V+ mass spectrometer. Precision on total C and N contents was better than 5% based on repeated analyses of a urea standard.

### 3.2.3 Stable sulfur isotopes

Stable sulfur isotope ratios were measured in hydrothermal sediments from the Barite field at Loki's Castle to identify past microbial activity. A few grams of sediment were collected at different depths from blade core GS18-28-BC3 and gravity core GS14-GC14 and dried at room temperature. Sulfide was subsequently extracted from ca. 20 mg of dried sediment using the hot chromium distillation method (Canfield et al., 1986), and precipitated as silver sulfide ($Ag_2S$). The fraction of sulfide represents chromium-reducible sulfide (CRS) as no significant amount of acid-volatile sulfide (AVS) was detected during the first acidification step. $Ag_2S$ was converted at the University of Münster into sulfur hexafluoride ($SF_6$) and subsequently purified by cryogenic and chromatographic methods (Farquhar et al., 2000), after which $SF_6$ was introduced into a ThermoScientific MAT 253 mass spectrometer via a dual-inlet system. Sulfur isotope data are reported relative to the Vienna Canyon Diablo Troilite (V-CDT) and calculated assuming vales of $\delta^{34}S$ = -0.300‰ and $\delta^{33}S$ = -0.055‰ for the IAEA-S1 standard, using Equations 5, 6 below:

$$\delta^{34}S = 1000\,[(^{34}S/^{32}S_{sample})/(34S/^{32}S_{V-CDT}) - 1] \quad (5)$$

$$\Delta^{33}S = \delta^{33}S - 1000\,[(1 + \delta^{34}S/1000)^{0.515} - 1] \quad (6)$$

10.3389/fmars.2023.1320655

The accuracy was monitored using reference standard IAEA-S1, yielding a precision (2s) of 0.09‰ for $\delta^{34}S$ and 0.017‰ for $\Delta^{33}S$.

# 4 Results

## 4.1 Kolbeinsey Ridge

Microbial sulfate reduction was not detected in marine sediments sampled at the Kolbeinsey Ridge (Figure 3A, Supplementary Table S1A). These sediments are characterized by low TOC values of 0.2-0.6 wt.%, an average C/N ratio of 2.58 (Supplementary Table S3), and pore fluid sulfate concentrations that are close to seawater values (28.5 mM; Baumberger et al., 2016b) with no significant downcore variation (Figure 4A, Supplementary Table S2A). Ammonium ($NH_4^+$) and methane ($CH_4$) are absent from pore waters, and alkalinity increases from 2.7 mM to slightly higher values (3-4 mM) at 200 cm depth. A hydrothermal chimney sample collected from the anhydrite-sulfide rich Lily mound in the Seven Sisters vent field yielded a sulfate reduction rate of 69 ± 34 pmol $SO_4^{2-}$ $cm^{-3}$ $d^{-1}$ (Figure 3C).

## 4.2 Mohns Ridge

Similar to the Kolbeinsey Ridge, no evidence was found for microbial sulfate reduction in marine sediments from the southern and central Mohns Ridge (Figure 3A) Total organic carbon contents and C/N ratios are comparably low, and range from 0.2-0.6 wt.% TOC and C/N = 3.13 at the southern Mohns Ridge, to 0.2-1.0 wt.% TOC and C/N = 4.80 at the central Mohns Ridge (Figures 4B, C). None of the sediment cores display pore water sulfate concentrations that are distinctly different from seawater values. Ammonium is absent in marine sediments from the southern Mohns Ridge (GS14-GC4), although this core displays the strongest increase in alkalinity from the seawater value (2.3 mM) at the top to 6.5 mM at 237 cm depth (Figure 4B). At the central Mohns Ridge, $NH_4^+$ appears at a depth of ~200 cm and increases to a value of 35 µM at 3.5 meters below the seafloor (GS14-GC8) with a corresponding change in alkalinity from 2.7 to 3.5 mM. No $CH_4$ was detected in the pore fluids. In contrast to the marine sediments, hydrothermal sediments (Figure 3B) and the high-temperature hydrothermal chimney Bruse (Figure 3C) from the Perle & Bruse venting area on the southern Mohns Ridge yield measurable sulfate reduction rates of 112 and 541 ± 116 pmol $cm^{-3}$ $d^{-1}$, respectively (Supplementary Table S1B, S1C).

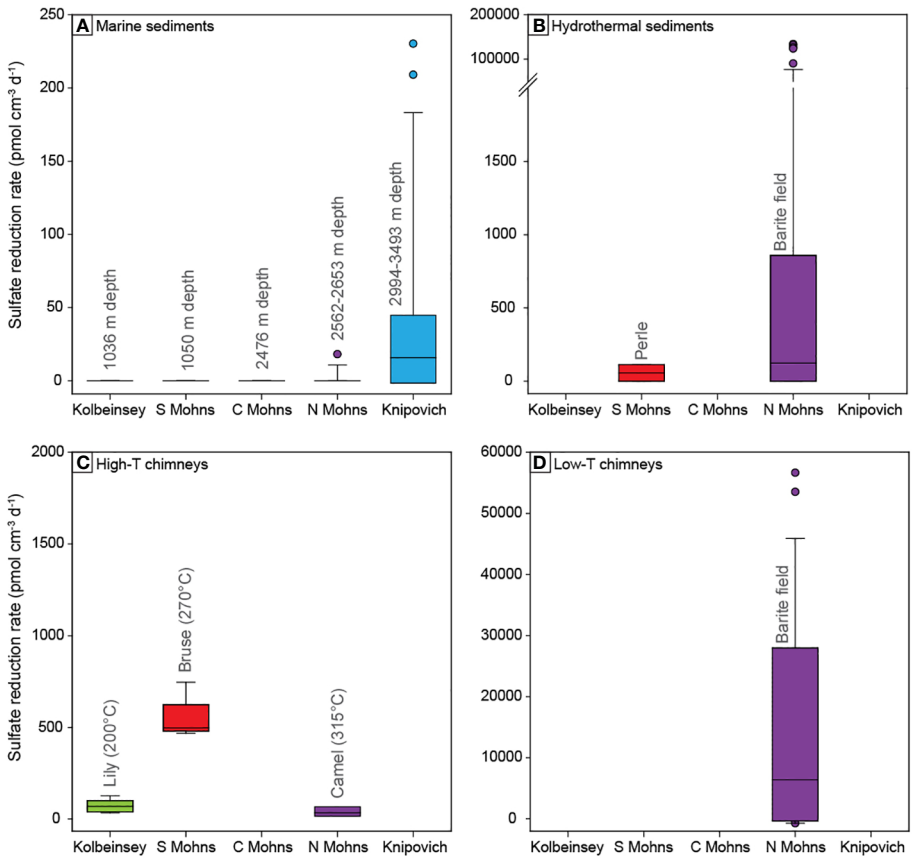


FIGURE 3
Box plots displaying sulfate reduction rates measured along the five segments of the AMOR. Panels reflect **(A)** marine sediments, **(B)** hydrothermal sediments, **(C)** high-temperature hydrothermal chimneys, **(D)** low-temperature hydrothermal chimneys. Note different scales for the y-axes. The highest sulfate reduction rates along the AMOR were measured in hydrothermal sediments from the Barite field.

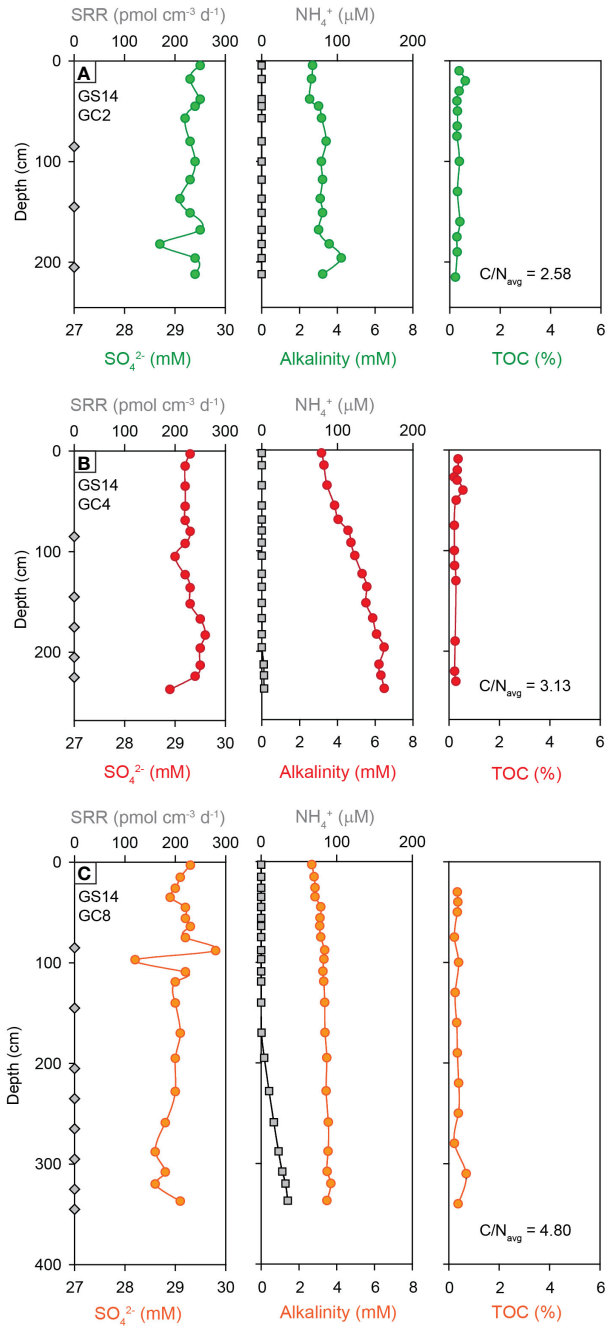


FIGURE 4
Depth profiles of sulfate reduction rates, pore fluid geochemistry ($SO_4^{2-}$, $NH_4^+$, alkalinity), total organic carbon (TOC) and average C/N ratios in marine sediment cores from the southern sections of the AMOR, with **(A)** Kolbeinsey Ridge, **(B)** Southern Mohns Ridge, **(C)** Central Mohns Ridge. Note that all sulfate reduction rates were below the detection limit in sediments from the southern AMOR.

Marine sediments from the northern Mohns Ridge (Figure 3A) show a similar absence of detectable microbial sulfate reduction as the southern sections of the Arctic Mid Ocean Ridge system, except for one horizon (380 cm) in sediments from the Bear Island Fan (GS15-GC1) where a rate of 18 pmol $SO_4^{2-}$ $cm^{-3}$ $d^{-1}$ was measured (Figure 5). This core also shows a downcore decrease in $SO_4^{2-}$ concentration, paired with an increase in $NH_4^+$ and alkalinity, as well as high TOC values of 5-8 wt.% in the bottom of the core (Figure 5). Methane was not detected.

The highest sulfate reduction rates in this study were measured in hydrothermal sediments (Figure 3B) and barite chimneys (Figure 3D) from the low-temperature Barite field at Loki's Castle, northern Mohns Ridge (Supplementary Tables S1B, S1C). Barite chimneys with visible venting and white microbial mats yield a maximum rate of 14633 pmol $SO_4^{2-}$ $cm^{-3}$ $d^{-1}$, but the variation in rates is significant between duplicate samples as well as the two different chimneys (average 3805 ± 5228 pmol $cm^{-3}$ $d^{-1}$). Yellow-colored barite chimneys display higher rates than the white mat-covered chimneys, with an average of 31267 ± 17209 pmol $cm^{-3}$ $d^{-1}$ (Figure 6). In contrast, the chimneys that are orange-colored yield a low rate of 205 ± 143 pmol $cm^{-3}$ $d^{-1}$, versus 929 ± 92 pmol $cm^{-3}$ $d^{-1}$ for white-colored chimneys with microbial mats (Figure 6). A rate of 39 ± 29 pmol $cm^{-3}$ $d^{-1}$ was obtained from the high-temperature sulfide chimney of Camel at Loki's Castle (Figure 3C).

A rate of 110478 pmol $cm^{-3}$ $d^{-1}$ was measured in a surface sediment layer between barite chimneys (GS15-9-PC2), and rates of 14828 to 93064 pmol $cm^{-3}$ $d^{-1}$ were found in sediments at 1-15 cm depth below a microbial mat (GS18-28-BC3) (Figure 7). These surface sediments are characterized by high TOC (6.6 wt.%), and pore water with high alkalinity (5.0 mM), $CH_4$ (185 nM), $H_2S$ (2555 μM) and $NH_4^+$ (1255 μM) (Supplementary Table S2B). Sulfur isotopic compositions of sulfide from sample GS18-28-BC3 range from $\delta^{34}S$ = 6.10 to 11.60‰, with positive $\Delta^{33}S$ values of 0.029 to 0.044‰ (Supplementary Table S4). The sulfate concentration in this horizon (21.5 mM) is significantly lower than seawater. In contrast, sediments from the gravity core (GS14-GC14) show much lower sulfate reduction rates, ranging from 3 to 93 pmol $cm^{-3}$ $d^{-1}$ in the upper 120 cm (Figure 7). No sulfate reduction rates were detected from 120 cm to 200 cm depth in the core, and sulfate concentrations are close to seawater (27.9-28.5 mM). Sulfide and methane are detected in pore fluids at concentrations of 7.3-32.4 μM $H_2S$ and 1.3-13.1 μM $CH_4$. Sulfide sulfur isotope ratios range from $\delta^{34}S$ = -3.74 to -21.68‰ with positive $\Delta^{33}S$ values of 0.021 to 0.138‰ (Supplementary Table S4).

## 4.3 Knipovich Ridge

Marine sediments from the Knipovich Ridge yield measurable sulfate reduction rates (Figure 8). The highest rates (up to 230 pmol $cm^{-3}$ $d^{-1}$) were detected in sediments within the rift valley (GS16-GC7), and lower rates of 13-89 pmol $cm^{-3}$ $d^{-1}$ were found in sediments on the eastern and western rift flanks. The Knipovich Ridge sediments are also geochemically distinct from the southern sections of the AMOR, with relatively high TOC values of 0.2-2.2 wt.% and an average C/N ratio of 5.74 ± 1.94, with the highest TOC and C/N measured in the rift valley (1.3 wt.% and 6.88 ± 0.30, respectively). The Knipovich sediments are also characterized by the presence of $NH_4^+$ just below the sediment-water interface (Figure 8), and alkalinity profiles show an increase from seawater alkalinity to values of 3.1-4.5 mM at depth at these locations. Methane was only detected in marine sediments at the Knipovich Ridge and ranges from 10 to 105 nM.

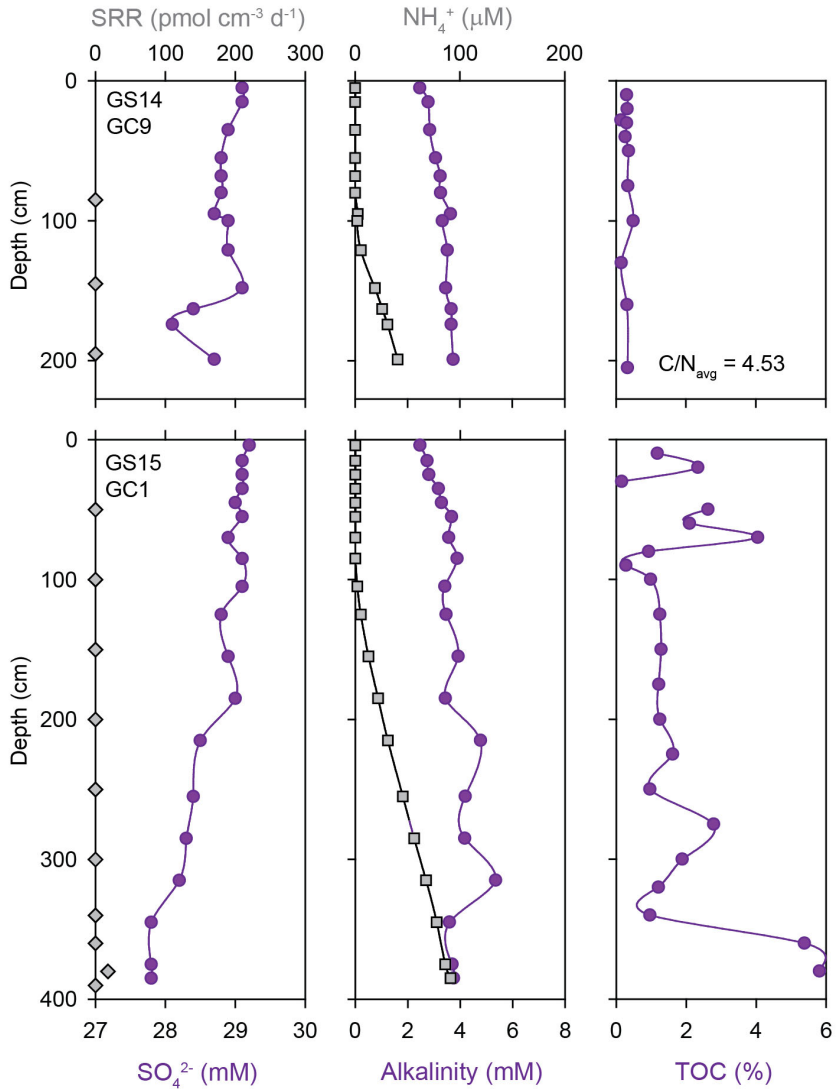


FIGURE 5
Depth profiles of sulfate reduction rates, pore fluid geochemistry ($SO_4^{2-}$, $NH_4^+$, alkalinity), total organic carbon (TOC) and average C/N ratios in marine sediment cores from the Northern Mohns Ridge. Note that only one sub-sample had a measurable sulfate reduction rate.

# 5 Discussion

## 5.1 Limited microbial sulfate reduction in deep marine sediments

Data presented in this paper expand the record of microbial sulfate reduction rates in the Arctic and confirm the relative insignificance of this metabolic pathway in the uppermost sediments of the deep marine realm in this region (cf. Bowles et al., 2014; Egger et al., 2018). Except for one horizon in core GS15-GC1, none of the marine sediment cores from the Kolbeinsey and Mohns Ridges yielded measurable gross sulfate reduction rates (Figure 3A) or showed significant changes in alkalinity coupled to decreasing sulfate concentrations in pore fluids (Figures 4, 5), indicating an absence of organoclastic sulfate reduction (OSR) and sulfate reduction coupled to anaerobic oxidation of methane (SR-AOM) in the upper 2-3 m of sediment (cf. Fossing et al., 2000; Gieskes et al., 2005; Jørgensen and Parkes, 2010; Wurgaft et al., 2019). This finding is not surprising given the low organic matter contents of the sediments (0.2-0.6 wt.% TOC) due to the relatively low sedimentation rates in the area (2-7 cm/1000 years) (Stein, 1990), and the degraded nature of this organic carbon as indicated by measured C/N ratios below that of marine plankton in Arctic regions (C/N ~ 6) (Martiny et al., 2013) (Figure 4, Figure 5). Such low-reactivity organic carbon has been shown to suppress sulfate reduction rates (Toth and Lerman, 1977; Goldhaber and Kaplan, 1975; Westrich and Berner, 1984), and as a result mineralization of organic carbon by sulfate reducers is not expressed in the studied sediments. Instead, increasing total alkalinity in core GS14-GC4 can be explained by the production of $HCO_3^-$ during higher energy-yielding microbial metabolisms in oxic and suboxic zones, including aerobic degradation of organic matter and microbial oxidation of generated ammonium ($NH_4^+$) by nitrification (Zhao et al., 2021). Similarly, the $NH_4^+$ profiles in cores GS14-GC8, GS14-

10.3389/fmars.2023.1320655

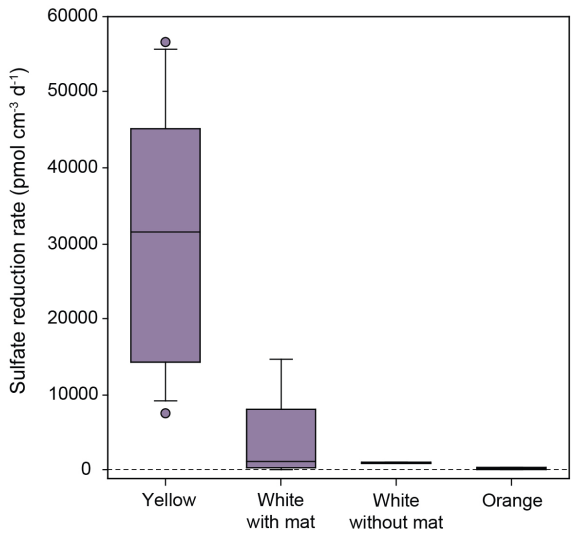


FIGURE 6
Box plots displaying sulfate reduction rates measured in low-temperature barite chimneys in the Loki's Castle Barite field on the Northern Mohns Ridge. Actively venting chimneys with a microbial mat show lower sulfate reduction rates than yellow chimneys without observable venting.

GC9 and GS15-GC1 are indicative of turnover of organic carbon, potentially related to iron and manganese reduction. The only non-zero sulfate reduction rate measured at 380 cm depth in GS15-GC1 may be related to the anomalously high TOC values of 6-8 wt.% at the base of this core (Figure 5), possibly reflecting variations in sedimentary sources during deposition of the glacigenic Bear Island Fan (Laberg and Vorren, 1996).

In contrast to the southern segments of the AMOR, sulfate reduction was detected in marine sediments from the Knipovich Ridge (Figure 3A). The low rates (13-230 pmol $cm^{-3}$ $d^{-1}$) lead to only minor changes in pore fluid sulfate concentrations and alkalinity with depth (Figure 8) and highlight the importance of radiotracer measurements to detect sulfate reduction in these sediments. We hypothesize that the occurrence of microbial sulfate reduction in the upper sediment layers of the Knipovich Ridge is best explained by a higher abundance of reactive organic matter. Although the Knipovich Ridge is the deepest section of the AMOR in this study (2994-3493 m), sediments have relatively high organic carbon contents of up to 2.2 wt.% TOC compared to a global average of 0.3 wt.% for deep marine settings (Rullkötter, 2006). In addition, measured C/N ratios of up to 6.88 (Figure 8) indicate that this organic matter is less degraded than on the Kolbeinsey and Mohns Ridges, and higher values on the eastern ridge flank (C/N = 3.7-13.6) than the western flank (C/N = 2.1-8.8) suggest that this is related to a supply of organic matter from coastal areas around Svalbard, located ca. 150 km east of the spreading ridge. Higher labile organic matter contents lead to shallower suboxic and anoxic zones, as shown by pore fluid ammonium profiles which demonstrate that oxygen penetrates less deeply into the sediments from the Knipovich Ridge than elsewhere along the AMOR (cf. Zhao et al., 2020). As a result, organoclastic sulfate reduction can be detected in the uppermost studied Knipovich

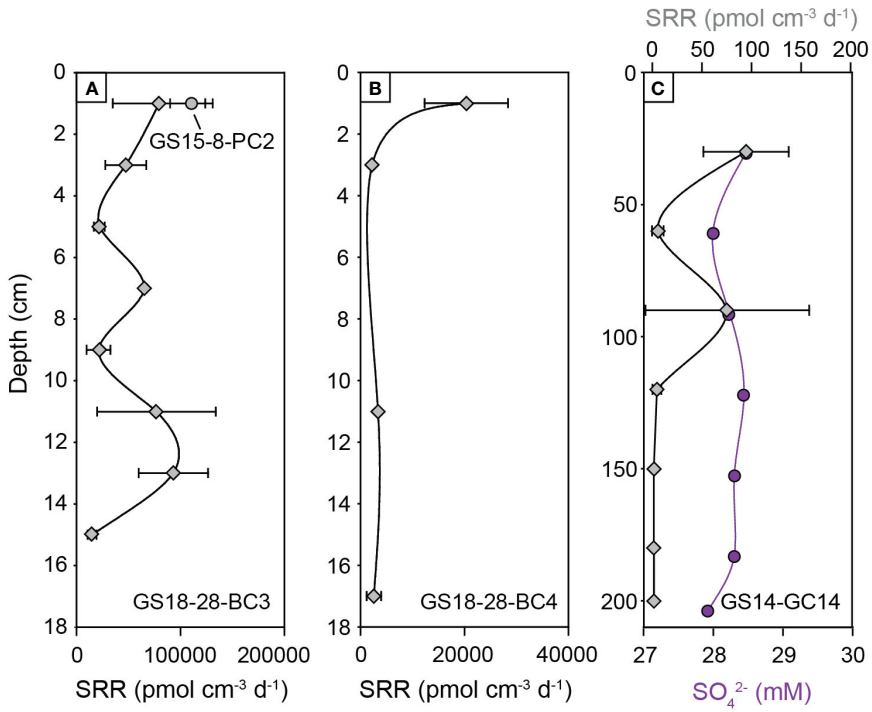


FIGURE 7
Depth profiles of sulfate reduction rates in hydrothermal sediments from the Loki's Castle Barite field, with **(A)** push core GS15-8-PC2 and blade core GS18-28-BC3 from actively venting sediments; **(B)** blade core GS18-28-BC4 from the perimeter of the Barite field; **(C)** gravity core GS14-GC14 from inside the Barite field, with pore fluid sulfate concentrations. Note the different scales for sulfate reduction rates.

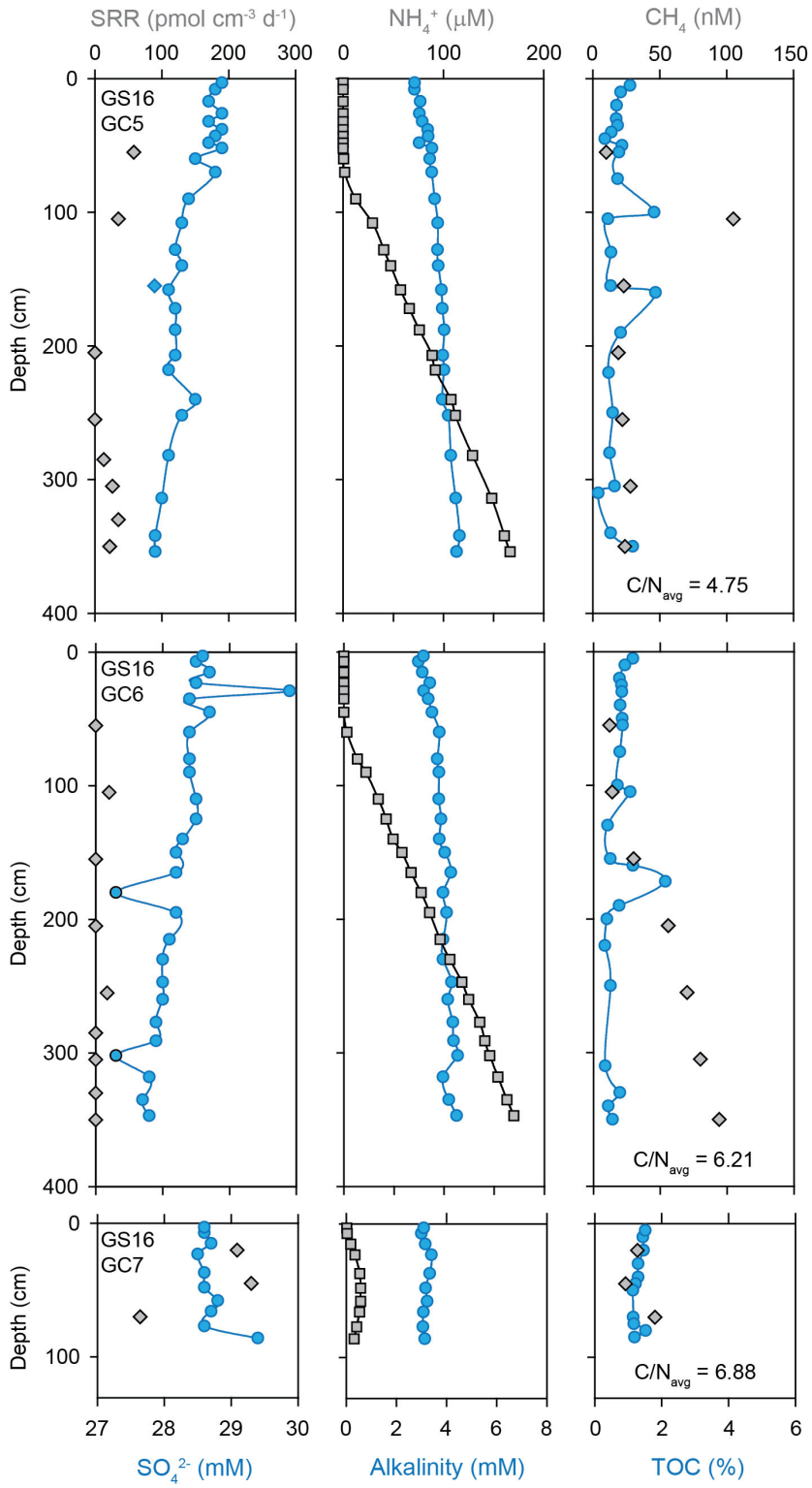


FIGURE 8
Depth profiles of sulfate reduction rates, pore fluid geochemistry ($SO_4^{2-}$, $NH_4^+$, alkalinity, $CH_4$), total organic carbon (TOC) and average C/N ratios in marine sediment cores from the Knipovich Ridge. In contrast to the southern AMOR segments, low but measurable sulfate reduction rates were obtained from all three sediment cores.

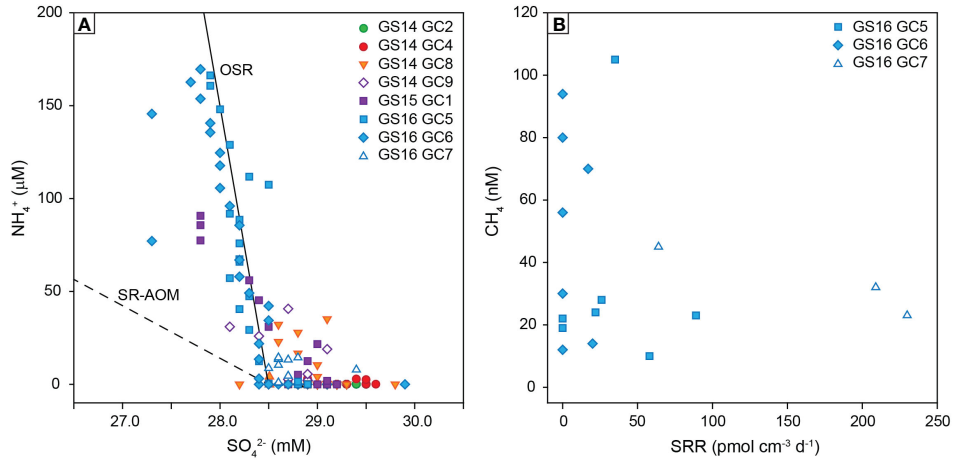


FIGURE 9
Trends in pore fluid geochemistry in marine sediments along the AMOR. **(A)** Pore fluid $NH_4^+$ versus $SO_4^{2-}$, with the dashed line displaying the trend associated with sulfate reduction coupled to anaerobic methane oxidation, and the solid line indicating organoclastic sulfate reduction (OSR) (Redfield et al., 1963; Greinert et al., 2002). Sediment cores from the Knipovich Ridge match with the trend predicted for OSR. **(B)** Pore fluid $CH_4$ versus sulfate reduction rates for sediment cores on the Knipovich Ridge, showing no correlation between methane and sulfate consumption.

Ridge sediments despite the large water depth (Figure 9A). Low levels of methane were also detected in pore fluids (Figure 8), but methane does not appear to be an electron donor for sulfate reducers in the studied Knipovich Ridge sediments, as evidenced by relatively high pore fluid $NH_4^+$ concentrations compared to $SO_4^{2-}$ (Figure 9A) and a lack of correlation between $CH_4$ and sulfate reduction rates (Figure 9B).

Our results thus demonstrate that microbial sulfate reduction is near-absent in the uppermost marine sediments investigated along the AMOR, most likely due to a limited availability of reactive organic matter in the distal parts of the ridge system that results in an extension of the oxic and suboxic zones beyond sampled sediment depths. The anoxic sulfate reduction zone was only detected in upper sediment layers from the Knipovich Ridge, where sedimentary influence from nearby Svalbard presumably results in higher electron donor availability and a more condensed redox zonation. However, rates are several orders of magnitude lower than measured in the shallow fjords on the west coast of Svalbard range (1 to 240 nmol $SO_4^{2-}$ $cm^{-3}$ $d^{-1}$) (Sagemann et al., 1998; Ravenschlag et al., 2000; Arnosti and Jørgensen, 2006; Michaud et al., 2020). Next, we compare these findings from background marine sediments with microbial sulfate reduction rates in three different hydrothermal settings on the AMOR.

## 5.2 Microbial sulfate reduction in basalt-hosted hydrothermal vent fields

We find evidence for microbial sulfate reduction in all high-temperature iron sulfide-rich hydrothermal chimneys from the basalt-hosted Seven Sisters, Jan Mayen and Loki's Castle vent fields, albeit at different rates (Figure 3C). The maximum measured rate in the Bruse chimney is about six times higher than for the Lily mound despite comparable experimental conditions such as incubation time and temperature (20°C), and more than one order of magnitude higher than the highest rate observed at Camel (incubated at 80°C). Frank et al. (2013) observed similar rate differences between venting deposits at Middle Valley and suggested that these variations are due to distinct biomass and microbial community composition, resulting from differences in substrate availability and physicochemical conditions. Distinct environments also provide a plausible explanation for the different rates at Lily and Bruse as the Seven Sisters vent field occurs at a shallower depth, has lower fluid $CH_4$ concentrations (Table 1), and hosts an ecosystem with abundant anemones, unlike the Bruse vent (Olsen et al., 2016). In contrast, the rates obtained for the Camel chimney at Loki's Castle more likely reflect the activity of archaeal and thermophilic sulfate reducers at 80°C, instead of mesophilic bacterial sulfate reduction targeted at Lily and Bruse with an incubation temperature of 20°C. The low rates are consistent with the absence of sulfate-reducing archaea *Archaeoglobus* and low relative abundance (<0.1%) of thermophilic sulfate reducers (*Thermodesulfobacteriaceae* and *Desulfohalobiaceae*) in our samples from Camel (Babel, 2019), but contradict with data from other chimneys at Loki's Castle that indicate relatively abundant (10-35%) sulfate-reducing micro-organisms in chimney walls (Vulcano et al., 2022). The low measured sulfate reduction rates at Camel thus most likely result from the sampling of chimney material where the temperature was not optimal for thermophilic sulfate reduction. For example, strong differences in the abundance of thermophilic sulfate reducers were reported between interior and exterior chimney walls (Jaeschke et al., 2012), implying that measured rates are highly dependent on the relative amount of chimney interior in the incubated slurries. This could also explain why we observe significant variations between replicates from individual chimneys (Figure 3C) (cf. Frank et al., 2013; Frank et al., 2015), and underscores the caution that should be exerted when extrapolating sulfate reduction rate data to other chimneys in a vent field.

Regardless of the microbial communities targeted in our incubation experiments, our results provide clear evidence for

microbial sulfate reduction in the basalt-hosted high-temperature venting areas on the AMOR. All high-temperature chimney sulfate reduction rates are higher than the zero background values measured in nearby marine sediment cores (Figure 3A). The inferred importance of the hydrothermal vent systems for microbial sulfate reduction is consistent with the general abundance of electron donors in these settings, including $CH_4$ and $H_2$ derived from vent fluids and organic compounds produced by chemoautotrophs and vent fauna (Jannasch and Mottl, 1985; Blake and Hilbig, 1990; McCollom and Shock, 1997; Alain et al., 2002; Sievert and Vetriani, 2012). For the investigated vent fields, energy landscape modeling predicts that organic carbon from primary production is the main electron donor for sulfate reducers (Dahle et al., 2015; Dahle et al., 2018), which is consistent with the detection of organotrophic sulfate reduction from our rate measurements that were performed for all samples in this study without the addition of $CH_4$ or $H_2$.

Interestingly, sulfate reduction rates from the AMOR high-temperature (200-315°C) hydrothermal chimneys are several orders of magnitude lower than rates reported from chimneys in other hydrothermal vent fields. Frank et al. (2013) measured rates of 355 to 6675 nmol $cm^{-3}$ $d^{-1}$ at 90°C (converted using a density of 2.5 g $cm^{-3}$) in high-temperature (123-261°C) chimneys from the sediment-hosted Middle Valley vent field on the Juan de Fuca Ridge, and similar average rates of 41 to 675 nmol $cm^{-3}$ $d^{-1}$ were obtained at 4 and 50°C from a hydrothermal flange (215°C) on the nearby sediment-influenced Main Endeavour Vent (Frank et al., 2015). Although the lower rates could be partly due to sampling of heterogeneous material as outlined above, we find consistently low sulfate reduction rates in chimneys from all three AMOR hydrothermal vent fields. Different experimental conditions, for example no addition of dissolved organic carbon or incubation below (20°C) or above (80°C) optimum temperatures, may also result in measured sulfate reduction rates that are lower than *in situ* rates. However, this is unlikely to explain the five orders of magnitude lower rates in our study, as previous experimental work suggests a much less strong dependency of rates on variables such as temperature (Frank et al., 2015). Relatively low metal concentrations in the Arctic vent fluids (Baumberger et al., 2016b; Marques et al., 2020) also argue against suppression of microbial sulfate reduction by toxic effects of dissolved metals (Frank et al., 2015). Instead, we hypothesize that the difference in sulfate reduction rates between chimneys on the AMOR and the Juan de Fuca Ridge may be related to the nature of the hydrothermal vent fields. Sedimented hydrothermal systems such as Middle Valley are characterized by fluids with higher $CH_4$ concentrations than basalt-hosted vent fields such as Seven Sisters and Jan Mayen, which would fuel sulfate reduction coupled to the anaerobic oxidation of methane as well as methanotrophy producing organic carbon for organoheterotrophic sulfate reducers in anaerobic niches (Nakamura and Takai, 2014). In contrast, chemosynthetic primary production in hydrothermal vent fields on sediment-free spreading ridges is dominated by aerobic sulfur and hydrogen oxidation in and on chimney walls (McCollom and Shock, 1997; Nakamura and Takai, 2014; Meier et al., 2017). However, further work on a more extensive sample set from the AMOR, in particular the sediment-influenced Loki's Castle vent field, is required to confirm this hypothesis.

## 5.3 High sulfate reduction rates in low-temperature hydrothermal areas

The highest sulfate reduction rates along the AMOR were measured in low-temperature barite chimneys and hydrothermal sediments from the Barite field at Loki's Castle (Figure 3). Rates of up to 55 nmol $SO_4^{2-}$ $cm^{-3}$ $d^{-1}$ in barite chimneys and 110 nmol $SO_4^{2-}$ $cm^{-3}$ $d^{-1}$ in the diffuse venting sediments at 2300 m depth (Figure 3D) are similar to sulfate reduction rates measured in coastal sediments around Svalbard at shallow water depths of 50-300 m (1-240 nmol $SO_4^{2-}$ $cm^{-3}$ $d^{-1}$) (Sagemann et al., 1998; Ravenschlag et al., 2000; Arnosti and Jørgensen, 2006; Michaud et al., 2020), and are exceptionally high for deep marine settings (cf. Bowles et al., 2014 and this study). However, our results agree well with sulfate reduction rates reported from hydrothermal sediments on the Juan de Fuca Ridge, with rates of 30 to 1563 nmol $SO_4^{2-}$ $cm^{-3}$ $d^{-1}$ measured in organic-rich hydrothermal sediments at Guaymas Basin (Jørgensen et al., 1990; Elsgaard et al., 1994) and 100 nmol $SO_4^{2-}$ $cm^{-3}$ $d^{-1}$ in metalliferous sediments at the Middle Valley hydrothermal vent field (Wankel et al., 2012). Observation of high sulfate reduction rates in the Barite field is also consistent with previous geochemical and microbiological studies that identified an important role for sulfate reducers in this low-temperature hydrothermal area (Eickmann et al., 2014; Jaeschke et al., 2014; Steen et al., 2016; Eickmann et al., 2020).

Possible substrates for sulfate reducers in the Barite field include organic compounds derived from microbial mats and vent fauna as well as methane supplied by low-temperature hydrothermal fluids. High sulfate reduction rates in sediments directly below a microbial mat with chemolithoautotrophic sulfur oxidizers (GS18-28-BC3; Vulcano et al., 2022) suggest an important role for organic matter production at the sediment-water interface. Similarly, supply of organic carbon from siboglinid tubeworms living at the sediment surface (Kongsrud and Rapp, 2012) explains high sulfate reduction rates in hydrothermal surface sediments with a total organic carbon content of 6.6 wt.% (GS15-8-PC2), as well as the sharp decrease in sulfate reduction rates with depth in sediments collected from the periphery of the Barite field (GS18-28-BC4) (Figure 7B). Organoclastic sulfate reduction was also inferred by Eickmann et al. (2020) to be the main pathway of sulfate reduction in the Barite field, based on pore fluid $NH_4^+/SO_4^{2-}$ and carbon isotope ratios in two gravity cores. However, recent work has additionally identified an abundant population of methane-oxidizing ANME-1 archaea with sulfate reducers as partners in the hydrothermal sediments (Steen et al., 2016; Vulcano et al., 2022), and our pore fluid data provide tentative evidence for methane as an another important electron donor for sulfate reducers in the Barite field. The diffuse venting fluids in the Barite field are thought to represent mixing of Mg-free high-temperature hydrothermal fluids and seawater with 51.8 mM Mg (Baumberger et al., 2016b), producing sediment pore fluids with Mg concentrations below that of seawater (Eickmann et al., 2014). Assuming conservative mixing for

magnesium (Tivey, 2007), we calculate contributions of high-temperature fluids of 5-18% and use this to predict 0.5-2 mM $CH_4$ in the diffuse vent fluids, based on an average $CH_4$ concentration of 13.8 mM in the hydrothermal end-member (Baumberger et al., 2016b). Predicted values are significantly higher than $CH_4$ concentrations of 0.2 to 13 µM measured in the pore fluids and suggest a loss of methane in the subsurface (Figure 10). Since the largest relative depletion in $CH_4$ is associated with the highest sulfate reduction rate (GS15-8-PC2) and is concomitant with relative enrichment in pore fluid $H_2S$ and deficit in $SO_4^{2-}$, these findings are best explained by microbial sulfate reduction coupled to anaerobic methane oxidation. Depletions in $CH_4$ observed below the active sulfate reduction zone in GS14-GC14 most likely reflect the operation of these metabolic processes in the subsurface (cf. Eickmann et al., 2014).

Despite the general abundance of electron donors, sulfate reduction rates are highly heterogeneous in the Barite field. Rates measured in the gravity core (Figure 7C) are nearly three orders of magnitude lower than those measured in the hydrothermal surface sediments (Figure 7A), and yellow-colored barite chimneys show higher rates than white or orange ones (Figure 6). Similar heterogeneity was found in hydrothermal sediments at Guaymas Basin (Jørgensen et al., 1990; Elsgaard et al., 1994) and Middle Valley (Wankel et al., 2012) and is likely inherent to diffuse venting hydrothermal systems, where fluid flow is controlled by subsurface variations in permeability that result in variable physiochemical conditions and biological habitats (Scheirer et al., 2006; Lowell et al., 2015). Likewise, the observed heterogeneity in sulfate reducing activity in the different barite chimneys may be explained by the distinct microbial communities reported for yellow-colored chimneys, which have a higher biomass density and abundance of sulfate reducers than barite chimneys with white microbial mats (Jaeschke et al., 2014; Steen et al., 2016). It should be noted that previous work classified the yellow-colored barite chimneys as inactive and chimneys with white mats as active (Jaeschke et al., 2014; Steen et al., 2016), but our findings suggest that a revision of this terminology is required. Observation of the highest sulfate reduction rates in the yellow barite chimneys (Figure 6) suggests that electron donors are abundant, despite the lack of visible fluid venting. We speculate that these chimneys are not inactive but exhibit very slow diffuse venting that is difficult to observe, and that their yellow appearance may be the result of a different type of microbial mat than the sulfide-oxidizers present in the white mats on visibly venting chimneys (Steen et al., 2016). It remains to be seen what the electron donors are in the different types of barite chimneys, and if they are limited or absent in the orange and white barite chimneys with no microbial mats and low sulfate reduction rates (Figure 6).

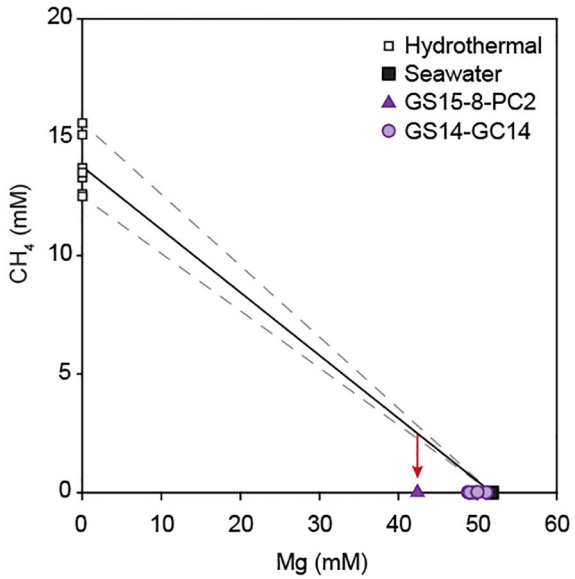


FIGURE 10
Concentration of $CH_4$ versus Mg in pore fluids from hydrothermal sediments in the Loki's Castle Barite field. The solid line indicates mixing between seawater and the average of end member hydrothermal fluids at Loki's Castle (Baumberger et al., 2016b), dashed lines are mixing lines with the highest and lowest values. The red arrow indicates that methane concentrations in the push core (GS15-8-PC2) and gravity core (GS14-GC14) are lower than expected based on mixing.

In addition to present-day microbial sulfate reduction inferred from our radiotracer incubations, multiple sulfur isotope data provide evidence that this metabolism has been active in the Barite field since the recent geological past. Sulfide minerals in the hydrothermal sediments show $\delta^{34}S$-values lower than ambient seawater ($\delta^{34}S$ = 21.2‰; Eickmann et al., 2014) and mostly fall onto mass relationships between $^{33}S/^{32}S$ and $^{34}S/^{32}S$ (defined as $^{33}\Lambda = \ln^{33}\alpha/\ln^{34}\alpha$) from 0.510 to 0.513 (Figure 11). These findings are consistent with major and minor sulfur isotope effects expected for microbial sulfate reduction (Harrison and Thode, 1958; Habicht and Canfield, 1997; Canfield, 2001; Detmers et al., 2001; Farquhar et al., 2003; Johnston et al., 2005; Johnston et al., 2007), and observation of the least $^{34}S$-depleted signatures in sediments with the highest sulfate reduction rates (GS18-28-BC3) agrees well with the predicted inverse correlation between magnitudes of isotope fractionation and sulfate reduction rates (Chambers et al., 1975; Jørgensen, 1979; Davidson et al., 2009; Leavitt et al., 2013). However, we also observe large shifts (25-40‰) in $\delta^{34}S$ relative to seawater in sediment horizons of the gravity core where no active microbial sulfate reduction was detected (156-200 cm; Figure 11). The isotopic composition of sulfides at 167 cm depth can be explained by the presence of Cu-Zn rich sulfide minerals that formed under high-temperature hydrothermal conditions, as suggested by its $^{33}\Lambda$-value of 0.515 that is indicative of a non-biological origin and a $\delta^{34}S$-value close to mantle-sulfur (~0‰) (Figure 11). In contrast, sulfur isotope ratios in sediments at 156 cm and 200 cm depth fall onto the mass relationship of $^{33}\Lambda \sim 0.513$ (Figure 11), which points to a microbial origin of sulfur isotope fractionation (cf. Farquhar et al., 2003; Johnston et al., 2007). The lack of measurable sulfate reduction rates at 156 and 200 cm (Figure 7C) indicates that these biogenic isotope effects are unrelated to current microbial activity, and must instead reflect microbial sulfate reduction before the present day. As such, the slightly lower pore fluid $SO_4^{2-}$ concentration at 200 cm depth (27.9

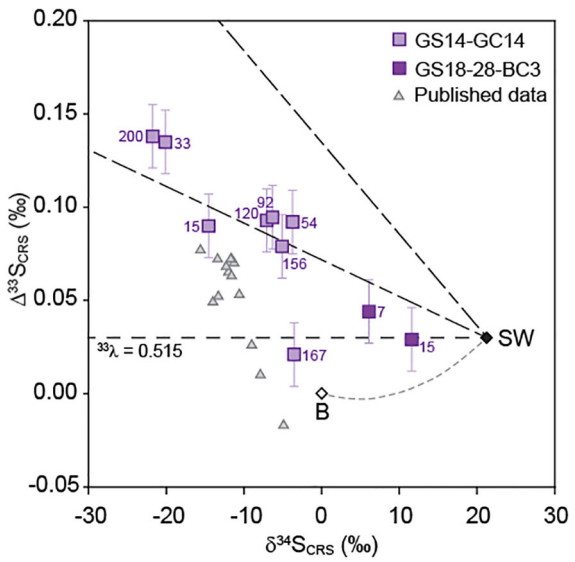


FIGURE 11
Multiple sulfur isotopic compositions of chromium-reducible sulfide (CRS) in blade core sediments (GS18-28-BC3) and gravity core sediments (GS14-GC14) from the Loki's Castle Barite field. Numbers next to symbols indicate core depths. Published data represent gravity cores from Eickmann et al. (2020). Dashed lines reflect isotope fractionation relative to seawater (SW) for different mass-relationships ($^{33}\Lambda$), with 0.510-0.513 reflecting microbial sulfate reduction (Farquhar et al., 2003; Johnston et al., 2007) and 0.515 high-temperature hydrothermal processes. Mixing between seawater (SW) and basalt (B) is also shown for reference. All $\Delta^{33}S$ values are calculated according to the definition in Equation 6 and error bars are 2σ.

mM) compared to seawater (Figure 7C) is more likely related to an increased contribution of sulfate-poor hydrothermal fluid rather than microbial consumption.

## 6 Conclusion

In this study, we demonstrate that hydrothermal activity can fuel microbial sulfate reduction in deep and distal marine settings on the AMOR that are otherwise characterized by insignificant sulfate reduction rates. Our findings confirm previous conclusions from sedimented and sediment-influenced hydrothermal systems on the Juan de Fuca Ridge that sulfate reduction is an important sulfur metabolism in hydrothermal settings in addition to sulfide oxidation (Jørgensen et al., 1990; Elsgaard et al., 1994; Kallmeyer and Boetius, 2004; Wankel et al., 2012; Frank et al., 2013; Frank et al., 2015), and further expand this to basalt-hosted hydrothermal vent fields. Microbial sulfate reduction is likely supported by an increased supply of electron donors, including organic compounds from primary producers in and on hydrothermal chimneys and vent fauna, as well as methane provided by high-temperature fluids. This is most clearly expressed in hydrothermal sediments and low-temperature barite chimneys from the Barite field at Loki's Castle, where high rates of up to 110 nmol $cm^{-3}$ $d^{-1}$ were measured and a relative depletion in pore fluid methane was observed. Although these results have limited implications for global sulfate reduction rates as the total surface area of hydrothermal vent fields is small compared to the entire ocean floor, our work indicates that the impact of microbial sulfate reduction on the local geochemistry of hydrothermal systems may be significant, in particular for sulfur and carbon cycling. For example, based on our highest measured sulfate reduction rate in hydrothermal sediments, contributions from sulfate reducers to diffuse venting fluids of the Barite field could be up to 10s of moles of sulfide per day. Further quantification of the impact of sulfate reducers on hydrothermal geochemistry requires improved estimates of vent fluxes, but importantly must consider the heterogeneity observed in sulfate reduction rates in the hydrothermal samples in our study.

## Data availability statement

The original contributions presented in the study are included in the article/Supplementary Material. Further inquiries can be directed to the corresponding author.

## Author contributions

DR: Conceptualization, Investigation, Methodology, Writing – original draft. FV: Investigation, Writing – review & editing. J-KL: Investigation, Writing – review & editing. KM: Investigation, Writing – review & editing. HB: Investigation, Writing – review & editing. SJ: Investigation, Writing – review & editing. TB: Investigation, Writing – review & editing. IØ: Investigation, Writing – review & editing. ER: Investigation, Writing – review & editing. IT: Funding acquisition, Investigation, Writing – review & editing. LR: Methodology, Writing – review & editing. HS: Investigation, Writing – review & editing. IS: Funding acquisition, Investigation, Supervision, Writing – review & editing.

## Funding

The author(s) declare financial support was received for the research, authorship, and/or publication of this article. This study was funded by the Research Council of Norway through the Centre for Geobiology, the K.G. Jebsen Foundation, the Trond Mohn Foundation and University of Bergen through the Centre for Deep Sea Research (grant no. TMS2020TMT13).

## Acknowledgments

We thank the captain and crew of R/V G.O. Sars, the pilots of ROV Ægir 6000 and cruise leader Rolf Birger Pedersen for their assistance in sample collection. Thibaut Barreyre is thanked for providing bathymetry data from Loki's Castle. Hildegunn Almelid, Pål Tore Mørkved, Anita-Elin Fedøy and Evy Foss Skjoldal are thanked for their technical assistance and geochemical analyses. We thank Dave Butterfield and two reviewers for their constructive comments that helped to improve this manuscript. This study was

funded by the Research Council of Norway through the Centre for Geobiology, the K.G. Jebsen Foundation, the Trond Mohn Foundation and University of Bergen through the Centre for Deep Sea Research (grant no. TMS2020TMT13). This is PMEL contribution 5556.

## Conflict of interest

The authors declare that the research was conducted in the absence of any commercial or financial relationships that could be construed as a potential conflict of interest.

## Publisher's note



## Supplementary material

The Supplementary Material for this article can be found online at: https://www.frontiersin.org/articles/10.3389/fmars.2023.1320655/full#supplementary-material

## References

Alain, K., Olagnon, M., Desbruyères, D., Pagé, A., Barbier, G., Juniper, S. K., et al. (2002). Phylogenetic characterization of the bacterial assemblage associated with mucous secretions of the hydrothermal vent polychaete Paralvinella palmiformis. *FEMS Microbiol. Ecol.* 42, 463–476. doi: 10.1111/j.1574-6941.2002.tb01035.x

Arnosti, C., and Jørgensen, B. B. (2006). Organic carbon degradation in arctic marine sediments, svalbard: a comparison of initial and terminal steps. *Geomicrobiology J.* 23, 551–563. doi: 10.1080/01490450600897336

Babel, H. R. (2019). *Metabolic properties of the hyperthermophilic sulfate reducing archaea of the genus Archaeoglobus in deep-sea hydrothermal vent systems, Department of Biological Sciences* (Norway: University of Bergen).

Baker, E. T., Edmonds, H. N., Michael, P. J., Bach, W., Dick, H. J., Snow, J. E., et al. (2004). Hydrothermal venting in magma deserts: The ultraslow-spreading Gakkel and Southwest Indian Ridges. *Geochemistry Geophysics Geosystems* 5. doi: 10.1029/2004GC000712

Baumberger, T., Früh-Green, G. L., Dini, A., Boschi, C., van Zuilen, K., Thorseth, I. H., et al. (2016a). Constraints on the sedimentary input into the Loki's Castle hydrothermal system (AMOR) from B isotope data. *Chem. Geology* 443, 111–120. doi: 10.1016/j.chemgeo.2016.09.026

Baumberger, T., Früh-Green, G. L., Thorseth, I. H., Lilley, M. D., Hamelin, C., Bernasconi, S. M., et al. (2016b). Fluid composition of the sediment-influenced Loki's castle vent field at the ultra-slow spreading Arctic Mid-Ocean ridge. *Geochimica Cosmochimica Acta* 187, 156–178. doi: 10.1016/j.gca.2016.05.017

Beaulieu, S. E., and Szafranski, K. (2020) *InterRidge global database of active submarine hydrothermal vent fields, version 3.4*. Available at: http://vents-data.interridge.org.

Berner, R. A. (1978). Sulfate reduction and the rate of deposition of marine sediments. *Earth Planetary Sci. Lett.* 37 (3), 492–498. doi: 10.1016/0012-821X(78)90065-1

Blake, J. A., and Hilbig, B. (1990). Polychaeta from the vicinity of deep-sea hydrothermal vents in the eastern Pacific. II. New species and records from the Juan de Fuca and Explorer Ridge systems. *Pac. Sci.* 44v (3), 219–253.

Bowles, M. W., Mogollón, J. M., Kasten, S., Zabel, M., and Hinrichs, K.-U. (2014). Global rates of marine sulfate reduction and implications for sub–sea-floor metabolic activities. *Science* 344, 889–891. doi: 10.1126/science.1249213

Bruvoll, V., Breivik, A. J., Mjelde, R., and Pedersen, R. B. (2009). Burial of the Mohn-Knipovich seafloor spreading ridge by the Bear Island Fan: Time constraints on tectonic evolution from seismic stratigraphy. *Tectonics* 28. doi: 10.1029/2008TC002396

Canfield, D. E. (1991). Sulfate reduction in deep-sea sediments. *Am. J. Sci.* 291, 177–188. doi: 10.2475/ajs.291.2.177

Canfield, D. E. (2001). Isotope fractionation by natural populations of sulfate-reducing bacteria. *Geochimica Cosmochimica Acta* 65, 1117–1124. doi: 10.1016/S0016-7037(00)00584-6

Canfield, D. E., Raiswell, R., Westrich, J. T., Reaves, C. M., and Berner, R. A. (1986). The use of chromium reduction in the analysis of reduced inorganic sulfur in sediments and shales. *Chem. Geology* 54, 149–155. doi: 10.1016/0009-2541(86)90078-1

Cannat, M., Fontaine, F., and Escartin, J. (2010). "Serpentinization and associated hydrogen and methane fluxes at slow spreading ridges," in *Diversity of hydrothermal systems on slow spreading ocean ridges*. Eds. P. A. Rona, C. W. Devey, J. Dyment and B. J. Murton (Washington, DC: AGU), 241–264.

Chambers, L. A., Trudinger, P. A., Smith, J. W., and Burns, M. S. (1975). Fractionation of sulfur isotopes by continuous cultures of Desulfovibrio desulfuricans. *Can. J. Microbiol.* 21, 1602–1607. doi: 10.1139/m75-234

Dahle, H., Le Moine Bauer, S., Baumberger, T., Stokke, R., Pedersen, R. B., Thorseth, I. H., et al. (2018). Energy landscapes in hydrothermal chimneys shape distributions of primary producers. *Front. Microbiol.* 9, 1570. doi: 10.3389/fmicb.2018.01570

Dahle, H., Økland, I., Thorseth, I. H., Pederesen, R. B., and Steen, I. H. (2015). Energy landscapes shape microbial communities in hydrothermal systems on the Arctic Mid-Ocean Ridge. *ISME J.* 9, 1593–1606. doi: 10.1038/ismej.2014.247

Davidson, M. M., Bisher, M., Pratt, L. M., Fong, J., Southam, G., Pfiffner, S. M., et al. (2009). Sulfur isotope enrichment during maintenance metabolism in the thermophilic sulfate-reducing bacterium Desulfotomaculum putei. *Appl. Environ. Microbiol.* 75, 5621–5630. doi: 10.1128/AEM.02948-08

Detmers, J., Bruchert, V., Habicht, K. S., and Kuever, J. (2001). Diversity of sulfur isotope fractionations by sulfate-reducing prokaryotes. *Appl. Environ. Microbiol.* 67, 888–894. doi: 10.1128/AEM.67.2.888-894.2001

Dick, H. J., Lin, J., and Schouten, H. (2003). An ultraslow-spreading class of ocean ridge. *Nature* 426, 405–412. doi: 10.1038/nature02128

Ding, J., Zhang, Y., Wang, H., Jian, H., Leng, H., and Xiao, X. (2017). Microbial community structure of deep-sea hydrothermal vents on the ultraslow spreading Southwest Indian Ridge. *Front. Microbiol.* 8, 1012. doi: 10.3389/fmicb.2017.01012

Edmonds, H., Michael, P., Baker, E., Connelly, D., Snow, J., Langmuir, C., et al. (2003). Discovery of abundant hydrothermal venting on the ultraslow-spreading Gakkel ridge in the Arctic Ocean. *Nature* 421, 252–256. doi: 10.1038/nature01351

Egger, M., Riedinger, N., Mogollón, J. M., and Jørgensen, B. B. (2018). Global diffusive fluxes of methane in marine sediments. *Nat. Geosci.* 11, 421–425. doi: 10.1038/s41561-018-0122-8

Eickmann, B., Baumberger, T., Thorseth, I. H., Strauss, H., Früh-Green, G. L., Pedersen, R. B., et al. (2020). Sub-seafloor sulfur cycling in a low-temperature barite field: A multi-proxy study from the Arctic Loki's Castle vent field. *Chem. Geology* 539, 119495. doi: 10.1016/j.chemgeo.2020.119495

Eickmann, B., Thorseth, I., Peters, M., Strauss, H., Bröcker, M., and Pedersen, R. (2014). Barite in hydrothermal environments as a recorder of subseafloor processes: a multiple-isotope study from the Loki's Castle vent field. *Geobiology* 12, 308–321. doi: 10.1111/gbi.12086

Elsgaard, L., Isaksen, M. F., Jørgensen, B. B., Alayse, A.-M., and Jannasch, H. W. (1994). Microbial sulfate reduction in deep-sea sediments at the Guaymas Basin hydrothermal vent area: influence of temperature and substrates. *Geochimica Cosmochimica Acta* 58, 3335–3343. doi: 10.1016/0016-7037(94)90089-2

Farquhar, J., Bao, H., and Thiemens, M. (2000). Atmospheric influence of earth's earliest sulfur cycle. *Science* 289, 756–758. doi: 10.1126/science.289.5480.756

Farquhar, J., Johnston, D. T., Wing, B. A., Habicht, K. S., Canfield, D. E., Airieau, S., et al. (2003). Multiple sulphur isotopic interpretations of biosynthetic pathways: implications for biological signatures in the sulphur isotope record. *Geobiology* 1, 27–36. doi: 10.1046/j.1472-4669.2003.00007.x

Fiedler, A., and Faleide, J. I. (1996). Cenozoic sedimentation along the southwestern Barents Sea margin in relation to uplift and erosion of the shelf. *Global Planet. Change* 12, 75–93. doi: 10.1016/0921-8181(95)00013-5

Fossing, H., Ferdelman, T. G., and Berg, P. (2000). Sulfate reduction and methane oxidation in continental margin sediments influenced by irrigation (South-East Atlantic off Namibia). *Geochimica Cosmochimica Acta* 64, 897–910. doi: 10.1016/S0016-7037(99)00349-X

Fossing, H., and Jørgensen, B. B. (1989). Measurement of bacterial sulfate reduction in sediments: evaluation of a single-step chromium reduction method. *Biogeochemistry* 8, 205–222. doi: 10.1007/BF00002889

Frank, K. L., Rogers, D. R., Olins, H. C., Vidoudez, C., and Girguis, P. R. (2013). Characterizing the distribution and rates of microbial sulfate reduction at Middle Valley hydrothermal vents. *ISME J.* 7, 1391–1401. doi: 10.1038/ismej.2013.17

Frank, K. L., Rogers, K. L., Rogers, D. R., Johnston, D. T., and Girguis, P. R. (2015). Key factors influencing rates of heterotrophic sulfate reduction in active seafloor hydrothermal massive sulfide deposits. *Front. Microbiol.* 6, 1449. doi: 10.3389/fmicb.2015.01449

Gieskes, J., Mahn, C., Day, S., Martin, J. B., Greinert, J., Rathburn, T., et al. (2005). A study of the chemistry of pore fluids and authigenic carbonates in methane seep environments: Kodiak Trench, Hydrate Ridge, Monterey Bay, and Eel River Basin. *Chem. Geology* 220, 329–345. doi: 10.1016/j.chemgeo.2005.04.002

Goldhaber, M. B., and Kaplan, I. R. (1975). Controls and consequences of sulfate reduction rates in recent marine sediments. *Soil Sci.* 119 (1), 42–55. doi: 10.1097/00010694-197501000-00008

Greinert, J., Bollwerk, S. M., Derkachev, A., Bohrmann, G., and Suess, E. (2002). Massive barite deposits and carbonate mineralization in the Derugin Basin, Sea of Okhotsk: precipitation processes at cold seep sites. *Earth Planetary Sci. Lett.* 203, 165–180. doi: 10.1016/S0012-821X(02)00830-0

Habicht, K. S., and Canfield, D. E. (1997). Sulfur isotope fractionation during bacterial sulfate reduction in organic-rich sediments. *Geochimica Cosmochimica Acta* 61, 5351–5361. doi: 10.1016/S0016-7037(97)00311-6

Harrison, A. G., and Thode, H. G. (1958). Mechanism of the bacterial reduction of sulphate from isotope fractionation studies. *Trans. Faraday Soc.* 53, 84–92. doi: 10.1039/tf9585400084

Horita, J., and Berndt, M. E. (1999). Abiogenic methane formation and isotopic fractionation under hydrothermal conditions. *Science* 285, 1055–1057. doi: 10.1126/science.285.5430.1055

Howarth, R. W., and Jørgensen, B. B. (1984). Formation of 35S-labelled elemental sulfur and pyrite in coastal marine sediments (Limfjorden and Kysing Fjord, Denmark) during short-term 35SO42– reduction measurements. *Geochimica cosmochimica Acta* 48, 1807–1818. doi: 10.1016/0016-7037(84)90034-6

Jaeschke, A., Eickmann, B., Lang, S. Q., Bernasconi, S. M., Strauss, H., and Früh-Green, G. L. (2014). Biosignatures in chimney structures and sediment from the Loki's Castle low-temperature hydrothermal vent field at the Arctic Mid-Ocean Ridge. *Extremophiles* 18, 545–560. doi: 10.1007/s00792-014-0640-2

Jaeschke, A., Jørgensen, S. L., Bernasconi, S. M., Pedersen, R. B., Thorseth, I. H., and Früh-Green, G. L. (2012). Microbial diversity of Loki's Castle black smokers at the Arctic Mid-Ocean Ridge. *Geobiology* 10, 548–561. doi: 10.1111/gbi.12009

Jannasch, H. W., and Mottl, M. J. (1985). Geomicrobiology of deep-sea hydrothermal vents. *Science* 229, 717–725. doi: 10.1126/science.229.4715.717

Johnston, D. T., Farquhar, J., and Canfield, D. E. (2007). Sulfur isotope insights into microbial sulfate reduction: When microbes meet models. *Geochimica Cosmochimica Acta* 71, 3929–3947. doi: 10.1016/j.gca.2007.05.008

Johnston, D. T., Farquhar, J., Wing, B. A., Kaufman, A. J., Canfield, D. E., and Habicht, K. S. (2005). Multiple sulfur isotope fractionations in biological systems: A case study with sulfate reducers and sulfur disproportionators. *Am. J. Sci.* 305, 645–660. doi: 10.2475/ajs.305.6-8.645

Jørgensen, B. B. (1979). A theoretical model of the stable sulfur isotope distribution in marine sediments. *Geochimica Cosmochimica Acta* 43, 363–374. doi: 10.1016/0016-7037(79)90201-1

Jørgensen, B. B. (1982). Mineralization of organic matter in the sea bed—the role of sulphate reduction. *Nature* 296 (5858), 643–645. doi: 10.1038/296643a0

Jørgensen, B. B., Findlay, A. J., and Pellerin, A. (2019). The biogeochemical sulfur cycle of marine sediments. *Front. Microbiol.* 10, 849. doi: 10.3389/fmicb.2019.00849

Jørgensen, B. B., and Kasten, S. (2006). "Sulfur cycling and methane oxidation," in *Marine geochemistry*. Eds. H. D. Schulz and M. Zabel (Berlin: Springer), 271–309.

Jørgensen, B. B., and Parkes, R. J. (2010). Role of sulfate reduction and methane production by organic carbon degradation in eutrophic fjord sediments (Limfjorden, Denmark). *Limnol. Oceanogr.* 55, 1338–1352. doi: 10.4319/lo.2010.55.3.1338

Jørgensen, B. B., Zawacki, L. X., and Jannasch, H. W. (1990). Thermophilic bacterial sulfate reduction in deep-sea sediments at the Guaymas Basin hydrothermal vent site (Gulf of California). *Deep Sea Res. Part A. Oceanographic Res. Papers* 37, 695–710. doi: 10.1016/0198-0149(90)90099-H

Kallmeyer, J., and Boetius, A. (2004). Effects of temperature and pressure on sulfate reduction and anaerobic oxidation of methane in hydrothermal sediments of Guaymas Basin. *Appl. Environ. Microbiol.* 70, 1231–1233. doi: 10.1128/AEM.70.2.1231-1233.2004

Kallmeyer, J., Ferdelman, T. G., Weber, A., Fossing, H., and Jørgensen, B. B. (2004). A cold chromium distillation procedure for radiolabeled sulfide applied to sulfate reduction measurements. *Limnology Oceanography: Methods* 2, 171–180. doi: 10.4319/lom.2004.2.171

Kelley, D. S., Karson, J. A., Blackman, D. K., FruÈh-Green, G. L., Butterfield, D. A., Lilley, M. D., et al. (2001). An off-axis hydrothermal vent field near the Mid-Atlantic Ridge at 30 N. *Nature* 412, 145–149. doi: 10.1038/35084000

Kinsey, J. C., and German, C. R. (2013). Sustained volcanically-hosted venting at ultraslow ridges: Piccard hydrothermal field, Mid-Cayman Rise. *Earth Planetary Sci. Lett.* 380, 162–168. doi: 10.1016/j.epsl.2013.08.001

Kongsrud, J. A., and Rapp, H. T. (2012). Nicomache (Loxochona) lokii sp. nov. (Annelida: Polychaeta: Maldanidae) from the Loki's Castle vent field: an important structure builder in an Arctic vent system. *Polar Biol.* 35, 161–170. doi: 10.1007/s00300-011-1048-4

Laberg, J. S., and Vorren, T. O. (1996). The middle and late pleistocene evolution and the bear island trough mouth fan. *Global Planet. Change* 12, 309–330. doi: 10.1016/0921-8181(95)00026-7

Leavitt, W. D., Halevy, I., Bradley, A. S., and Johnston, D. T. (2013). Influence of sulfate reduction rates on the Phanerozoic sulfur isotope record. *Proc. Natl. Acad. Sci.* 110, 11244–11249. doi: 10.1073/pnas.1218874110

Lecoeuvre, A., Ménez, B., Cannat, M., Chavagnac, V., and Gérard, E. (2021). Microbial ecology of the newly discovered serpentinite-hosted Old City hydrothermal field (southwest Indian ridge). *ISME J.* 15, 818–832. doi: 10.1038/s41396-020-00816-7

Lowell, R. P., Houghton, J. L., Farough, A., Craft, K. L., Larson, B. I., and Meile, C. D. (2015). Mathematical modeling of diffuse flow in seafloor hydrothermal systems: The potential extent of the subsurface biosphere at mid-ocean ridges. *Earth Planetary Sci. Lett.* 425, 145–153. doi: 10.1016/j.epsl.2015.05.047

Marques, A. F., Roerdink, D. L., Baumberger, T., de Ronde, C. E. J., Ditchburn, R. G., Denny, A., et al. (2020). The seven sisters hydrothermal system: first record of shallow hybrid mineralization hosted in mafic volcaniclasts on the arctic mid-ocean ridge. *Minerals* 10, 439. doi: 10.3390/min10050439

Martiny, A. C., Pham, C. T. A., Primeau, F. W., Vrugt, J. A., Moore, J. K., Levin, S. A., et al. (2013). Strong latitudinal patterns in the elemental ratios of marine plankton and organic matter. *Nat. Geosci.* 6, 279–283. doi: 10.1038/ngeo1757

McCollom, T. M., and Shock, E. L. (1997). Geochemical constraints on chemolithoautotrophic metabolism by microorganisms in seafloor hydrothermal systems. *Geochimica cosmochimica Acta* 61, 4375–4391. doi: 10.1016/S0016-7037(97)00241-X

Meier, D. V., Pjevac, P., Bach, W., Hourdez, S., Girguis, P. R., Vidoudez, C., et al. (2017). Niche partitioning of diverse sulfur-oxidizing bacteria at hydrothermal vents. *ISME J.* 11, 1545–1558. doi: 10.1038/ismej.2017.37

Michaud, A. B., Laufer, K., Findlay, A., Pellerin, A., Antler, G., Turchyn, A. V., et al. (2020). Glacial influence on the iron and sulfur cycles in Arctic fjord sediments (Svalbard). *Geochimica Cosmochimica Acta* 280, 423–440. doi: 10.1016/j.gca.2019.12.033

Moeslundi, L., Thamdrup, B., and Jørgensen, B. B. (1994). Sulfur and iron cycling in a coastal sediment: radiotracer studies and seasonal dynamics. *Biogeochemistry* 27, 129–152. doi: 10.1007/BF00002815

Nakamura, K., and Takai, K. (2014). Theoretical constraints of physical and chemical properties of hydrothermal fluids on variations in chemolithotrophic microbial communities in seafloor hydrothermal systems. *Prog. Earth Planetary Sci.* 1, 1–24. doi: 10.1186/2197-4284-1-5

Olsen, B. R., Økland, I. E., Thorseth, I. H., Pedersen, R. B., and Rapp, H. T. (2016). *Environmental challenges related to offshore mining and gas hydrate extraction* (Norway: Norwegian Environment Agency).

Pedersen, R. B., and Bjerkgård, T. (2016). Seafloor massive sulphides in Arctic waters. *Mineral Resour. In Arctic* 1, 209–216.

Pedersen, R. B., Rapp, H. T., Thorseth, I. H., Lilley, M. D., Barriga, F. J. A. S., Baumberger, T., et al. (2010a). Discovery of a black smoker vent field and vent fauna at the Arctic Mid-Ocean Ridge. *Nat. Commun.* 1, 126. doi: 10.1038/ncomms1124

Pedersen, R. B., Thorseth, I. H., Hellevang, B., Schultz, A., Taylor, P., Knudsen, H. P., et al. (2005). Two vent fields discovered at the ultraslow spreading Arctic Ridge System. *Eos Trans. AGU Fall Meet. Suppl.* 86. Abstract OS21C-01.

Pedersen, R. B., Thorseth, I. H., Nygård, T. E., Lilley, M. D., and Kelley, D. S. (2010b). "Hydrothermal activity at the Arctic mid-ocean ridges," in *Diversity of hydrothermal systems on slow spreading ocean ridges*. Eds. P. A. Rona, C. W. Devey, J. Dyment and B. J. Murton (Washington, DC: AGU), 67–89.

Ravenschlag, K., Sahm, K., Knoblauch, C., Jørgensen, B. B., and Amann, R. (2000). Community structure, cellular rRNA content, and activity of sulfate-reducing bacteria in marine arctic sediments. *Appl. Environ. Microbiol.* 66, 3592–3602. doi: 10.1128/AEM.66.8.3592-3602.2000

Redfield, A. C., Ketchum, B. H., and Richards, F. A. (1963). The Influence of Organisms on the Composition of the Sea Water. *The Sea* (New York: Interscience Publishers) 2, 26–77.

Røy, H., Weber, H. S., Tarpgaard, I. H., Ferdelman, T. G., and Jørgensen, B. B. (2014). Determination of dissimilatory sulfate reduction rates in marine sediment via radioactive 35S tracer. *Limnology Oceanography: Methods* 12, 196–211. doi: 10.4319/lom.2014.12.196

Rullkötter, J. (2006). "Organic matter: the driving force for early diagenesis," in *Marine geochemistry*, Eds. H. D. Schulz and M. Zabel (Berlin: Springer),125–168.

Sagemann, J., Jørgensen, B. B., and Greeff, O. (1998). Temperature dependence and rates of sulfate reduction in cold sediments of svalbard, arctic ocean. *Geomicrobiology J.* 15, 85–100. doi: 10.1080/01490459809378067

Scheirer, D. S., Shank, T. M., and Fornari, D. J. (2006). Temperature variations at diffuse and focused flow hydrothermal vent sites along the northern East Pacific Rise. *Geochemistry Geophysics Geosystems* 7. doi: 10.1029/2005GC001094

Seyfried, W. E. (1987). Experimental and theoretical constraints on hydrothermal alteration processes at mid-ocean ridges. *Annu. Rev. Earth Planetary Sci.* 15, 317–335. doi: 10.1146/annurev.ea.15.050187.001533

Sievert, S. M., and Vetriani, C. (2012). Chemoautotrophy at deep-sea vents: past, present, and future. *Oceanography* 25, 218–233. doi: 10.5670/oceanog.2012.21

Snow, J. E., and Edmonds, H. N. (2007). Ultraslow-spreading ridges rapid paradigm changes. *Oceanography* 20, 90–101. doi: 10.5670/oceanog.2007.83

Steen, I. H., Dahle, H., Stokke, R., Roalkvam, I., Daae, F.-L., Rapp, H. T., et al. (2016). Novel barite chimneys at the Loki's castle vent field shed light on key factors shaping microbial communities and functions in hydrothermal systems. *Front. Microbiol.* 6, 1510. doi: 10.3389/fmicb.2015.01510

Stein, R. (1990). Organic carbon content/sedimentation rate relationship and its paleoenvironmental significance for marine sediments. *Geo-Mar. Lett.* 10, 37–44. doi: 10.1007/BF02431020

Stubseid, H. H., Bjerga, A., Haflidason, H., Pedersen, L. E. R., and Pedersen, R. B. (2023). Volcanic evolution of an ultraslow-spreading ridge. *Nat. Commun.* 14, 4134. doi: 10.1038/s41467-023-39925-0

Tao, C., Lin, J., Guo, S., Chen, Y. J., Wu, G., Han, X., et al. (2012). First active hydrothermal vents on an ultraslow-spreading center: Southwest Indian Ridge. *Geology* 40, 47–50. doi: 10.1130/G32389.1

Thamdrup, B., Fossing, H., and Jørgensen, B. B. (1994). Manganese, iron and sulfur cycling in a coastal marine sediment, Aarhus Bay, Denmark. *Geochimica Cosmochimica Acta* 58, 5115–5129. doi: 10.1016/0016-7037(94)90298-4

Tivey, M. K. (2007). Generation of seafloor hydrothermal vent fluids and associated mineral deposits. *Oceanography* 20, 50–65. doi: 10.5670/oceanog.2007.80

Toth, D. J., and Lerman, A. (1977). Organic matter reactivity and sedimentation rates in the ocean. *Am. J. Sci.* 277, 465. doi: 10.2475/ajs.277.4.465

Vulcano, F., Hahn, C. J., Roerdink, D., Dahle, H., Reeves, E. P., Wegener, G., et al. (2022). Phylogenetic and functional diverse ANME-1 thrive in Arctic hydrothermal vents. *FEMS Microbiol. Ecol.* 98. doi: 10.1093/femsec/fiac117

Wankel, S. D., Adams, M. M., Johnston, D. T., Hansel, C. M., Joye, S. B., and Girguis, P. R. (2012). Anaerobic methane oxidation in metalliferous hydrothermal sediments: influence on carbon flux and decoupling from sulfate reduction. *Environ. Microbiol.* 14, 2726–2740. doi: 10.1111/j.1462-2920.2012.02825.x

Westrich, J. T., and Berner, R. A. (1984). The role of sedimentary organic matter in bacterial sulfate reduction: The G model tested. *Limnol. Oceanogr.* 29, 236–249. doi: 10.4319/lo.1984.29.2.0236

Wurgaft, E., Findlay, A. J., Vigderovich, H., Herut, B., and Sivan, O. (2019). Sulfate reduction rates in the sediments of the Mediterranean continental shelf inferred from combined dissolved inorganic carbon and total alkalinity profiles. *Mar. Chem.* 211, 64–74. doi: 10.1016/j.marchem.2019.03.004

Zhao, R., Mogollón, J. M., Abby, S. S., Schleper, C., Biddle, J. F., Roerdink, D. L., et al. (2020). Geochemical transition zone powering microbial growth in subsurface sediments. *Proc. Natl. Acad. Sci.* 117, 32617–32626. doi: 10.1073/pnas.2005917117

Zhao, R., Mogollón, J. M., Roerdink, D. L., Thorseth, I. H., Økland, I., and Jørgensen, S. L. (2021). Ammonia-oxidizing archaea have similar power requirements in diverse marine oxic sediments. *ISME J.* 15, 3657–3667. doi: 10.1038/s41396-021-01041-6